ABSTRACT

KRAJCOVIC, MATEJ. Leading Edge Dynamics during Spreading and Migration. (Under the direction of Jason M. Haugh).

Cell migration is an essential part of wound healing and cancer metastasis. Cells interpret adhesive and soluble stimuli from the environment into directed movement. During cell migration, cells protrude in the direction of motion, forming a leading edge, and retract at the trailing edge. The signaling events at the leading edge are crucial for efficient migration.

Cells bind to extracellular matrix (ECM) via integrin receptors. Phosphoinositide 3-kinase (PI3K) is activated in fibroblasts during spreading on fibronectin and poly-lysine. Blocking of integrin receptors by β1-integrin antibody inhibits adhesion on fibronectin but not on poly-lysine. PI3K activity is not affected by integrin blocking on poly-lysine. Active Rac, a Rho GTPase, stimulates formation of lamellipodia at the leading edge. We used fluorescent probes for Rac and PI3K in conjunction with total internal fluorescence microscopy (TIRF) to examine spatial distribution of Rac and PI3K. In randomly migrating fibroblasts, Rac and PI3K are co-localized most times in the cell protrusions.

The mechanisms governing the formation and disassembly of integrin-ECM adhesion complexes at the protruding leading edge are central to the understanding of cell migration. We have developed a simplified mathematical model that incorporates adhesion and protrusion dynamics mediated by Rac/Pak (p21-activated kinase) signaling at the leading edge. Nascent adhesions either disassemble (turn over) or mature into stable focal adhesions. Stable adhesions can be involved in two distinct pathways of protrusion inhibition. We performed a bifurcation analysis with respect to density of ECM and existence of two possible steady states has been shown. A stochastic version of the model employing the Gillepsie algorithm was developed to model the effect of diffusion in a linear geometry. At certain conditions, multiple states of activation are present within the leading edge.

Leading Edge Dynamics during Spreading and Migration

by
Matej Krajcovic

A thesis submitted to the Graduate Faculty of
North Carolina State University
in partial fulfillment of the
requirements for the Degree of
Master of Science

Chemical Engineering

Raleigh, North Carolina

July 2008

APPROVED BY:

_____	_____
David F. Ollis	Balaji Rao

_____

Jason M. Haugh
Chair of Advisory Committee

BIOGRAPHY

Matej Krajcovic was born in Bratislava, the capital city of Slovakia. He attended a high school with special emphasis on mathematics and physical sciences in his home town. He spent his senior year at Bucksport High School in Maine, where he was presented with the possibility of pursuing higher education in the USA. After completion of his high school in Slovakia, he enrolled at the University of Maine in the college of engineering. During his undergraduate years he had a chance to perform research, which solidified his intention to pursue graduate education. After receiving his bachelor's degree in chemical engineering he enrolled at North Carolina State University to pursue a graduate degree in the same major. After his first semester he joined the group of Dr. Jason Haugh.

ACKNOWLEDGEMENTS

My experience at North Carolina State University has been wonderful and truly memorable. I would first like to thank my advisor, Dr. Jason Haugh, for his guidance and support during my time here. I would also like to express my gratitude to my committee members, Dr. Balaji Rao and Dr. David Ollis. Learning how to conduct research in the laboratory would be a daunting task without the help of my lab mates. I would like to thank all the members of Haugh group, particularly Michael Weiger for teaching me the majority of techniques that I used for my master's thesis. Finally, I must thank my family and my girlfriend Sawyer for their unconditional love and support.

TABLE OF CONTENTS

LIST OF FIGURES

LIST OF TABLES

LIST OF ABBREVIATIONS

ATP – Adenosine Triphosphate
GAP – GTPase Activating Protein
GDI – GDP Dissociation Inhibitor
GEF – Guanine nucleotide Exchange Factor
GIT - G protein-coupled receptor kinase-interacting protein
ECM – Extracellular Matrix
EGFP – Enhanced Green Fluorescent Protein
FAK – Focal Adhesion Kinase
FN – Fibronectin
PDGF – Platelet Derived Growth Factor
PAK – p21 activated kinase
PI - Phosphoinositide
PI3K – Phosphoinositide 3-kinase
PIP_3 – 3'phosphoinositide
RGD - Arginine-Glycine-Aspartic acid sequence
TIRF – Total internal fluorescence microscopy

CHAPTER 1: Signaling at the leading edge

1.1 MOTIVATION

The processes of cell proliferation and cell migration require a complex signaling network to implement cues from inside of the cell as well as from the external environment. Cell migration is an essential part of wound healing and metastasis of cancer cells. Due to their complexity, signaling pathways responsible for these processes have not been completely elucidated.

A variety of research methods have been used to investigate the signaling networks within cells. The most robust method is to inhibit a particular pathway, and then observe the resulting phenotype or measure protein levels by western blotting. These experiments are important for elucidating the basic signaling interactions, but they are insufficient when more detail at the cell level is desired. Subcellular imaging with specific fluorescent probes allows the distribution of signaling molecules to be studied *in vivo*. Cells can be observed after fixation, or live in real time. Confocal and total internal reflection fluorescence (TIRF) microscopies are particularly useful for studying signaling events at the membrane, where most signaling processes are initiated. With a variety of fluorescent proteins available, it is possible to use different molecular probes to track multiple signaling molecules simultaneously (Shaner et al., 2004). This approach can yield invaluable insight into the interaction of different pathways and their localization within cells.

The advancement of computational technology in recent years has lead to wide use of mathematical modeling in the realm of cell biology. Data from classic experimental methods, such as protein blotting, can be implemented to build complex mathematical models which can be used to propose new experiments. Models with ordinary differential equations are suitable for average quantities in a cell population; however, a stochastic approach is more appropriate for single cell modeling, because the number of molecules can be quite low (< 100/cell).

1.2 BACKGROUND

1.2.1 Cell organization

Eukaryotic cells are only ~10 μm in size, yet they are very complex in structure. A cell contains a nucleus, cytoplasm, and the plasma membrane. Genetic material is stored in the nucleus. Cytoplasm has three major components: cytosol, organelles and cytoskeleton. Cytosol is a semi-clear liquid composed mostly of water, salts and organic molecules. Organelles are small compartments enclosed in a lipid membrane and perform various functions, such as ATP production (mitochondria) and protein synthesis (ribosomes). Cytoskeleton is a network of structural proteins that serves as scaffolding for the entire cell. Plasma membrane serves as a barrier between the cytoplasm and the extracellular environment.

Most processes important for cell migration occur at the plasma membrane or associated with the cytoskeleton. The plasma membrane contains numerous proteins, some of which serve as receptors for extracellular factors that transduce signals to the cytoplasm. The cytoskeleton is a dynamic structure that is controlled primarily by molecular assembly and disassembly.

1.2.2 Integrin receptors

Integrins are a family of cell surface receptors that mediate attachment to the extracellular matrix (ECM), cell-cell adhesive interactions, apoptosis, metastasis and the response of cells to mechanical stress (Clark and Brugge, 1995). Integrins are heterodimers of α and β subunits that span across the cell membrane. In mammals, 24 integrin types have been identified to date, resulting from different combination of 18 α- and 8 β-subunits (Arnaout et al., 2005; Berman et al., 2003). Each subunit contains three domains: a glycosylated extracellular domain, a hydrophobic transmembrane domain and a cytoplasmic domain. Attachment to extracellular matrix (ECM) is mediated through integrin recognition sites for short linear sequences, e.g. Arg-Gly-Asp (RGD), that are present in ECM proteins such as fibronectin (Schwartz et al., 1995). Integrins are not merely attachment proteins; they mediate signal transduction by both

"outside-in" or "inside-out" mechanisms. The cytoplasmic tails of intergrins are generally short and lack enzymatic activity. Hence, integrins transduce signals by associating with adaptor proteins that carry the signals to cytosol and cytoskeleton. As integrins bind to ECM they tend to cluster into focal adhesions, complexes that promote assembly of actin filaments. The reorganization of actin into stress fibers in turn promotes integrin clustering, creating a positive feedback loop (Giancotti and Ruoslahti, 1999).

1.2.3 Focal adhesions

New integrin adhesions to ECM are generally formed in the leading protrusive edges of the cell called lamellipodia. Initially, each adhesion occupies a small area (~0.25 μm^2) and recruits several adaptor proteins, such as paxillin and talin (Zamir and Geiger, 2001). These nascent focal adhesions can either disassemble (turn over) or mature into stable focal adhesions (Moissoglu and Schwarz, 2006). Maturation involves recruitment of more integrin receptors and association of the focal adhesion with actin bundles (Carragher and Frame, 2004). A fully formed, stable adhesion can contain more than 50 structural and signaling molecules (Zamir and Geiger, 2001).

When paxillin and talin are bound to the integrin receptor, they recruit focal adhesions kinase (FAK) and vinculin to the focal contacts. The protein α-actinin is phosphorylated by FAK, binds to vinculin and crosslinks actomyosin stress fibers and connects them to focal adhesions (Figure 1.1). Myosin is a motor protein, the function of which is described in more detail later in this Chapter. Other proteins commonly present in focal adhesions include the protein tyrosine kinase Src, the adaptor protein p130Cas, and the binding protein zyxin (Mitra et al., 2005). The composition of focal contacts changes dynamically in response to external cues and cellular behavior.

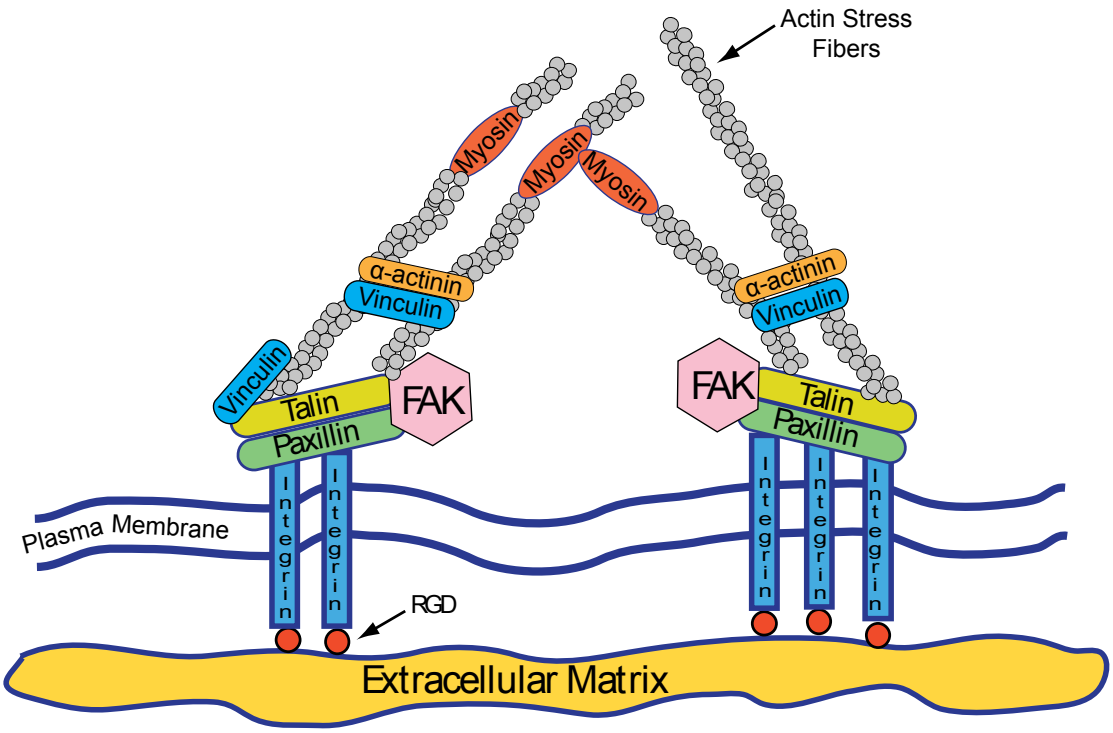

Figure 1.1 Focal adhesion complex. Integrins bind the RGD sequence in extracellular matrix and then recruit adaptor proteins talin and paxillin. FAK is recruited by to this complex and phosphorylates α-actinin, which binds actin fibers together. Myosin binds to actin fibers and causes them to move. The drawing is not to scale and numerous other proteins have been omitted for clarity.

1.2.4 Phosphoinositide 3-kinase (PI3K)

PI3Ks are enzymes that catalyze phosphorylation of the 3'-OH position of the inositol ring of phosphatidylinositols (PtdIns) (Vanhaesebroeck and Waterfield, 1999). A phosphorylated PtdIns is called a phosphoinositide (PI). The positions of the phosphate groups on the inositol ring are essential for functional roles of PIs in cells.

Members of the PI3K family are divided into three groups based on the lipid substrate they commonly phosphorylate (Leevers et al., 1999). Class I and III PI3Ks are heterodimers composed of regulatory and catalytic subunits. Class I PI3Ks are divided into class IA and class IB based on which specific subunits they contain. Class IA PI3Ks consist of a 110 kDa catalytic domain (p110) and a 85 kDa regulatory domain (p85) (Vanhaesebroeck et al., 2001). Platelet-derived growth factor (PDGF) receptor activated by binding PDGF recruits p85 of PI3K and induces a conformational change

that activates catalytic activity of PI3K (Shoelson et al., 1993). Active FAK in focal adhesions can also bind p85 via phosphorylated Tyr397 of FAK, which activates PI3K (Chen et al., 1996). A schematic of PI3K function is shown in Figure 1.2.

The most common substrate of PI3K class IA phosphorylation is $PI(4,5)P_2$ which yields $PI(3,4,5)P_3$ (also knows as PIP_3). The reverse reaction, conversion of PIP_3 to $PI(4,5)P_2$, is catalyzed by PTEN phosphatase. The balance between the forward and reverse reaction plays a key role in chemotaxis (Kolsch et al., 2008). PIP_3 can bind signaling molecules containing a pleckstrin homology (PH) domain and thereby recruits them to the membrane (Lemmon et al., 2002). Important signaling proteins containing PH domains include Akt family protein kinases, pleckstrin and many others (Haslam et al., 1993).

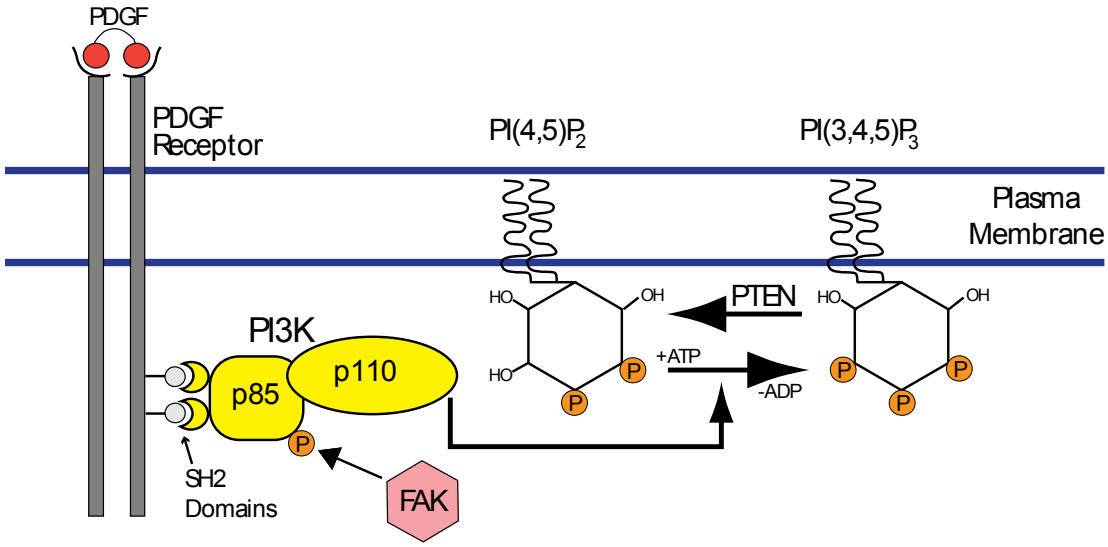

Figure 1.2 Function of PI3K. After PDGF receptor activation by PDGF, regulatory p85 domain of PI3K binds SH2 domains on PDGF receptor. Catalytic p110 domain of PI3K facilitates addition of phosphate group on 3' position of the inositol ring. The energy from this reaction comes from conversion ATP to ADP. The reverse reaction is catalyzed by PTEN phosphatase.

1.2.5 Rho GTPases

GTPases are molecular switches that cycle between an inactive, GDP-bound state and an active, GTP-bound state. While in the active state they recognize target proteins and generate responses until they are converted back to the inactive state (Etienne-Manneville and Hall, 2002). The activation of a GTPase is mediated by guanine nucleotide exchange factors (GEFs), whereas the reverse transition is by a GTP hydrolysis reaction that is accelerated by GTPase activating proteins (GAPs).

There are several hundred known GTPases in eukaryotic cells, but in this document we focus on a small family of Rho GTPases, because they play an important role in cytoskeleton dynamics (Figure 1.3). The best characterized members of this family are Rho, Rac and Cdc42. Rho regulates the assembly of focal adhesions and actin stress fibers (Ridley and Hall, 1992) . Basal Rho activity is also essential to maintain cell substrate adhesion (Ridley et al., 1995). Cdc42 triggers formation of finger-like protrusions called filopodia, and it is required to establish polarity during cell movement (Nobes and Hall, 1995; Nobes and Hall, 1999). Activity of Rac is essential for formation of large actin-rich protrusions called lamellipodia and for membrane ruffling (Nobes and Hall, 1999; Ridley et al., 1992).

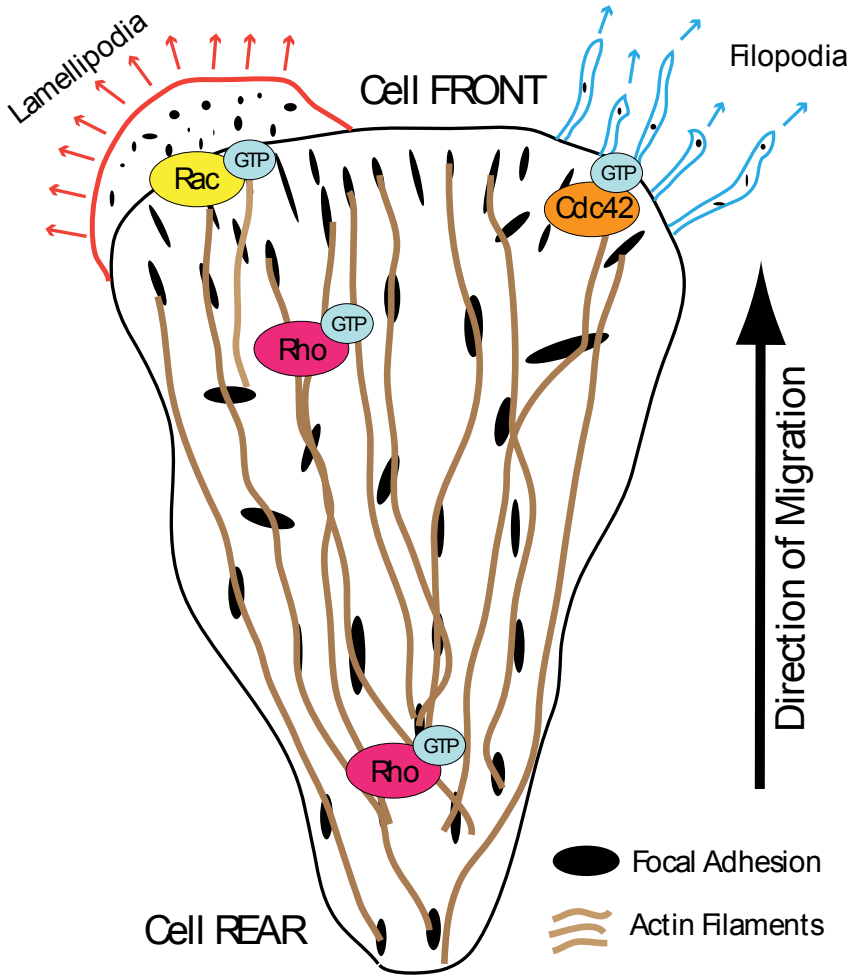

Figure 1.3 Rho-family GTPases. Cdc42, Rac and Rho are members of the Rho family GTPases and are active when bound to GTP. Cdc42 stimulates formation of finger like protrusions called filopodia that sense the environment for chemoattractants. Rac stimulates formation of large protrusion, lamellipodia where nascent focal adhesions are formed. Rho is involved in formation of actin stress fibers and formation of focal adhesions. The size of filopodia, lamellipodia and focal adhesions is exaggerated for clarity.

1.2.6 Rac

The small GTPase Rac interacts with a wide array of signaling molecules and is an important regulator of cell movement. Active Rac binds p85 subunit of PI3K *in vitro* and stimulates PI3K activity by 2-9 fold (Bokoch et al., 1996). This increase in PI3K activity in response to Rac binding is only a small fraction of total PI3K activity (Tolias et al., 1995). Several Rac-specific GEFs bind to the PI3K product PIP_3, raising the

possibility of a positive feedback loop between PI3K and Rac (Han et al., 1998; Welch et al., 2003).

The location of Rac molecules in cells depends on its activation state (Figure 1.4). When Rac is activated by GEFs, it is recruited to the membrane, but deactivation by GAPs releases it back to the cytosol. The sequestration of inactive Rac in the cytosol is attributed to its binding to the guanine-nucleotide dissociation inhibitor (GDI), Rho-GDI. The GAP-dependent conversion to Rac-GDP is apparently the rate-limiting step in this process (Moissoglu et al., 2006). Deletion of the Rac1 gene in mouse embryonic fibroblasts revealed a critical function of Rac in actin stress fiber formation and focal adhesion complex assembly. The Rac1-null fibroblasts did not exhibit lower levels or Rho, and overexpression of Rho failed to recover the actin stress fiber formation (Guo et al., 2006). During fibroblast migration after wounding, the highest levels of active Rac are observed at the leading edge (Kraynov et al., 2000). In motile neutrophils, high active Rac levels are present at the leading edge as well as in the retracting tail (Gardiner et al., 2002; Pestonjamasp et al., 2006).

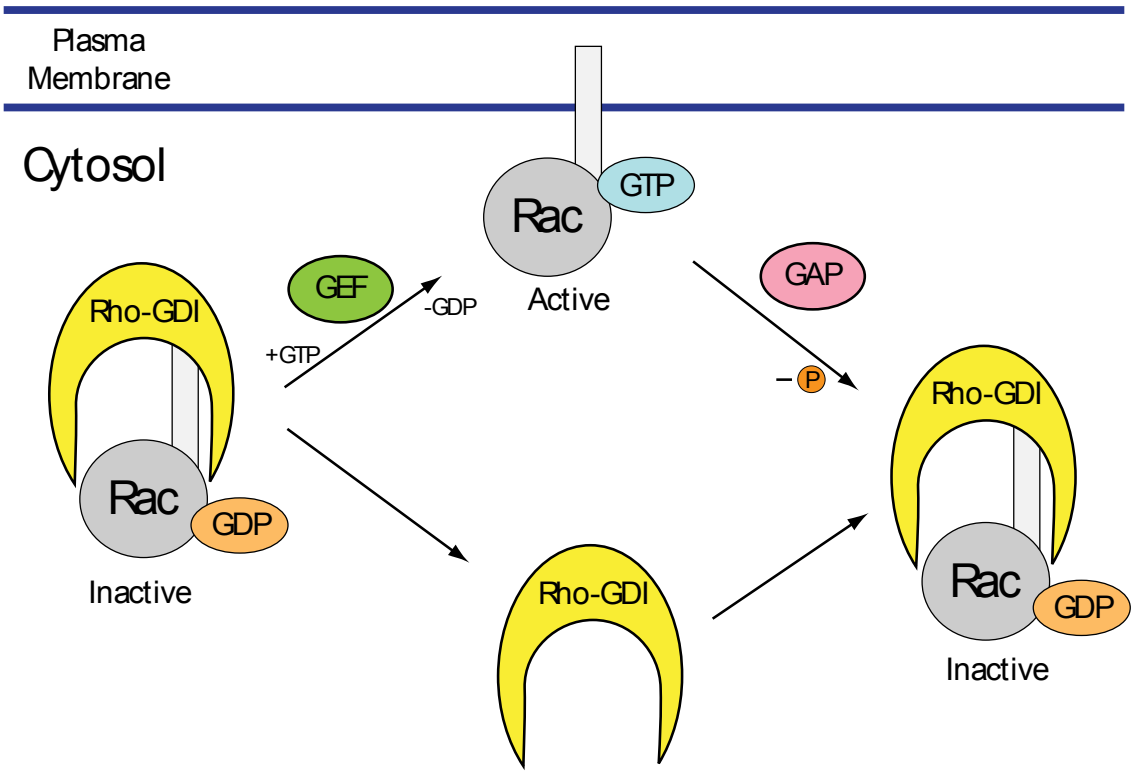

Figure 1.4 Activation and deactivation of Rac. Inactive, GDP-bound Rac is attached to Rho-GDI in the cytosol. Guanine nucleotide exchange factors (GEFs) facilitate the exchange of GDP with GTP on Rac, which leads to activation and translocation of Rac to the membrane. GTPase activating proteins stimulate removal of phosphate group from GTP resulting in inactivation of Rac and its binding to Rho-GDI.

1.2.7 Paxillin and GIT1-Pix-Pak complex

Paxillin is present in focal adhesion complexes and contains a number of protein motifs that serve as docking sites for cytoskeletal proteins, tyrosine kinases, serine/threonine kinases, GTPase activating proteins and adaptor proteins found in focal adhesions (Schaller, 2001). Genetically encoded paxillin conjugated with green fluorescent protein (GFP-paxillin) is often used to study focal adhesion dynamics in cells (Zamir et al., 2000). Paxillin is also involved in turnover of adhesions at the base of protrusions (Webb et al., 2004).

The serine/threonine kinase, p21-activated kinase (Pak), is an effector of Rac and an important regulator in adhesion dynamics. A dominant-negative mutant of Pak in endothelial cells increased stress fibers and focal adhesions (Kiosses et al., 1999). Phosphorylation of paxillin on serine 273 by Pak significantly increases migration,

protrusion and adhesion turnover by increasing binding of paxillin to G protein-coupled receptor kinase-interacting protein (GIT1). GIT1 and Pak interact with Pak-interactive exchange factor (Pix) to form the GIT1-Pix-Pak signaling complex. Paxillin phosphorylated at Ser273 by Pak stimulates the localization of this complex at the leading edge, thus constituting a positive feedback loop (Nayal et al., 2006).

1.2.8 Myosin

Myosin is a motor protein that interacts with actin to generate muscle contraction and other forms of cell motility (Craig and Woodhead, 2006). Different myosin proteins are grouped into 12 different classes based on their structure and function. Myosin II is the best characterized class, which actuates motility by moving actin (Sellers et al., 1996). Myosin II has two isoforms: IIA, which regulates actin retrograde flow, and IIB, which controls protrusion stability; both isoforms mediate stress fiber formation (Vicente-Manzanares et al., 2007).

Myosin II is an elongated, two-headed molecule consisting of two identical light chains and two pairs of heavy chains. The head domain binds actin filaments and generates force to "walk" along actin fibers by hydrolyzing ATP. The light chain connects the head and the heavy chain and contains regulatory regions. The heavy chain binds other heavy chains into myosin bundles (Craig and Woodhead, 2006).

The regulatory light chain of myosin II is readily phosphorylated by myosin light chain kinase but also to some extent by Pak (Chew et al., 1998). Active Pak also phosphorylates myosin light chain kinase (MLCK), resulting in decreased MLCK activity (Sanders et al., 1999). Since MLCK is the main regulator of MLC activity, these two effects of Pak are of a competitive nature. The small GTPase Rho activates Rho kinase, which phosphorylates myosin light chain and increases its activity (Burridge and Wennerberg, 2004).

In Chinese hamster ovary (CHO) cells, myosin II resides in regions that are distal from nascent focal adhesions, so its effect on adhesion dynamics is indirect. Adhesion maturation at the leading edge depends on the ATPase activities of both myosin II isoforms. Myosin II depletion increases cell protrusion and inhibits maturation of

nascent adhesions at the leading edge (Vicente-Manzanares et al., 2007). In mouse embryonic fibroblasts, myosin II is involved in traction force generation and retrograde F-actin flow. Depletion of myosin II results in a higher spreading rate and overall spreading area (Cai et al., 2006).

1.3 APPROACH

1.3.1 Total internal reflection fluorescence microscopy

The primary experimental technique used in this study is total internal reflection fluorescence (TIRF) microscopy. This technique was developed in 1980 by Daniel Alexrod and became widely used after development of genetically encoded enhanced green fluorescent protein (Axelrod, 1981; Heim et al., 1995). The main advantage of TIRF microscopy is its capability to excite only fluorophores near the cell membrane-substratum contact area, which results in excellent sensitivity and spatial resolution while minimizing photobleaching. Two designs are commonly used for TIRF microscopy: prism-based and objective-based (Axelrod, 2001). The setups differ in the way in which the excitation laser beam is delivered to the sample. In objective-based TIRF microscopy, which is used in all commercial, "off-the-shelf" TIRF microscopes, the objective guides the laser beam. We have utilized the prism-based approach, as described in more detail below (Figure 1.5).

In prism-based TIRF, a laser beam travels through a prism, where it is directed to the glass-aqueous interface on top of a glass cover slip, where the cells are adhered. The angle at which the beam encounters the interface is called the incidence angle, θ. If this angle is greater than the critical angle, the beam is reflected, and an evanescent wave is produced perpendicular to the glass-buffer interface. The intensity, I of the evanescent wave is a function of distance from the glass-buffer interface and is calculated as follows.

$$I = I_o e^{\frac{-d}{z}}; \qquad (1.1)$$

$$d = \frac{\lambda}{4\pi\sqrt{n_1^2 \sin^2\theta - n_2^2}}, \qquad (1.2)$$

where I_o is the intensity of the wave at the glass-buffer interface (z = 0), n_1 is the refractive index of glass, n_2 is the refractive index of the aqueous buffer, d is the characteristic decay depth, and λ is the excitation wavelength of the beam. The intensity of the evanescent wave decays exponentially with distance and effectively illuminates a height of only d ~ 100 nm above the interface. The cell membrane and signaling proteins near the membrane are present in this region, making TIRF microscopy an ideal method for observing their dynamics.

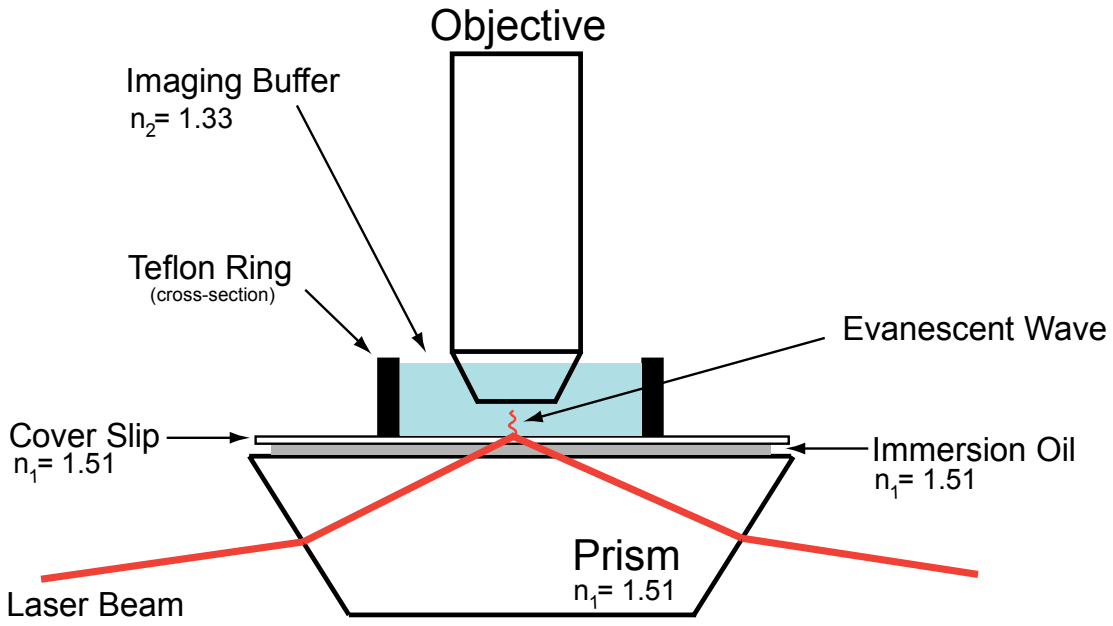

Figure 1.5 Experimental setup: TIRF Microscopy. Illustration of our experimental setup used for TIRF experiments with fibroblast cells expressing fluorescent proteins.

The visualization of signaling processes via genetically encoded fluorophores can be achieved in two different ways (Figure 1.6). Fluorescent proteins can be fused directly with the protein of interest, and this construct can be expressed in cells. For example, EGFP-tagged Rac and paxillin have been used to track their localization in living cells (Kraynov et al., 2000; Zamir et al., 2000). This method has well-known drawbacks. The expression of the tagged protein will result in a higher amount of the signaling protein than would be present in wild-type cells (the endogenous, untagged protein is still

present), which might affect the cellular response. Also, the fluorescent protein tag has a substantial mass, 27 kDa for EGFP, which might affect the protein function.

The second method of visualizing signal transduction is to use a biosensor that binds to the signaling protein or its immediate product. The biosensor consists of a fluorescent protein fused to a domain that binds the intracellular molecule of interest. The PH domain of Akt, fused to EGFP (or mCherry), binds reversibly to PIP_3, the product of PI3K activity. The distribution of this biosensor in cells is thus a suitable indicator of PI3K activity (Haugh et al., 2000). This biosensor does not directly affect the endogenous activity of PI3K, but it could affect the function of PIP_3 lipids if expressed at very high concentrations.

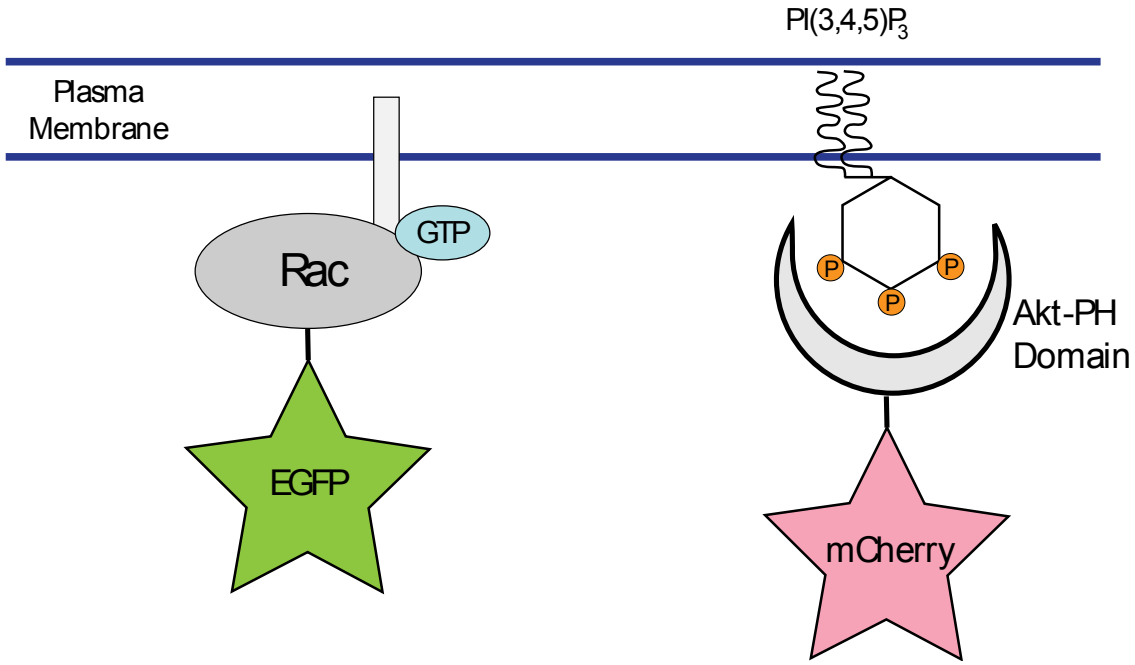

Figure 1.6 Examples of fluorescent biosensors for monitoring signal transduction. EGFP-Rac is a fusion protein of wild type Rac and EGFP. Biosensor for PI3K product PIP_3 is a fusion protein red fluorescent protein mCherry and Pleckstrin homology domain of Akt. While EGFP is covalently bonded to Rac, mCherry-AktPH binds reversibly to PIP_3.

1.3.2 Mathematical modeling

In recent years, the use of mathematical modeling and computational approaches has become more commonplace in the quest to understand the complexity of biological

systems. The advancement in computational technology in recent years made mathematical modeling a useful tool to study protein folding, signaling interactions, and other processes. Traditional models involve sets of ordinary or partial differential equations that describe levels of particular molecules in time and space. While this method is suitable for systems with large number of molecules, a stochastic model is more appropriate for systems with very small populations. Differential equations treat the system as a continuum, and the state variables represent species concentrations, whereas the stochastic approach treats changes in state as discrete events.

The most popular method for modeling stochastic, reacting systems in the time domain only is the Gillespie algorithm (Gillespie, 1976). In this algorithm, the system is expressed as a series of simple reactions, which change the numbers of participating species by one. In each loop, probabilities for all reactions are calculated based on the current population and parameters of the system. Randomly generated numbers are used to determine the time step and which reaction will occur. The advantages of the Gillespie algorithm are that it is exact and relatively easy to implement; however, unlike classic iterative differential equation solvers, it is inefficient in handling so-called stiff problems, which are characterized by a combination of very fast and very slow rate processes.

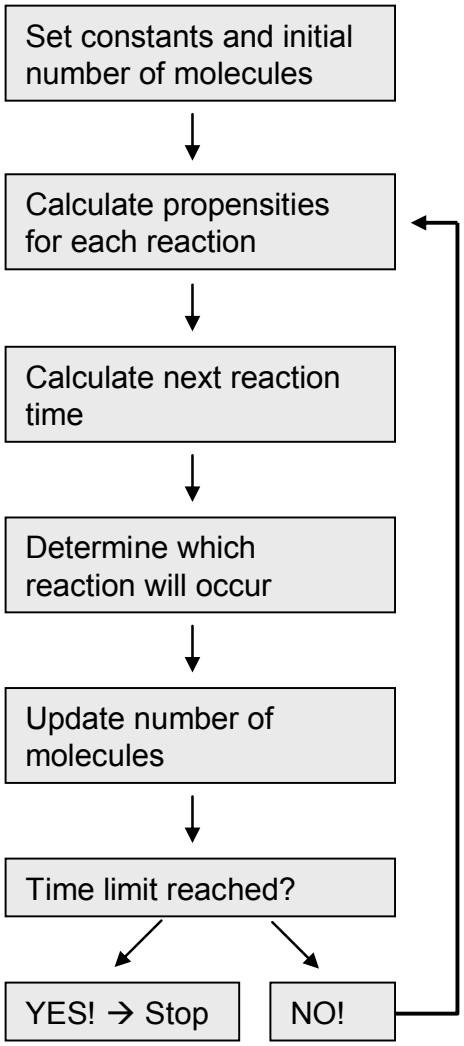

Figure 1.7 Gillespie algorithm. The steps are executed in the specified order by a computer. The algorithm is exact and stable because it determines the appropriate time step in each loop.

1.3.3 Goals of this study

Using TIRF microscopy in conjunction with fluorescent biosensors and mathematical modeling, we hope to address the following questions:

1. What is the spatial distribution of PI3K and Rac in randomly migrating fibroblasts? Is there any evidence of positive or negative feedback between the two? (Chapter 2)
2. Is the activation of PI3K during spreading mediated solely by integrin signaling? (Chapter 2)
3. What is the mechanism of integrin signaling at the leading edge? What is the mechanism behind wave-like behavior of Rac signaling and adhesion/protrusion dynamics in migrating cells? (Chapter 3)

1.4 REFERENCES

Arnaout, M., B. Mahalingam, and J. Xiong. 2005. Integrin structure, allostery, and bidirectional signaling. *ANNUAL REVIEW OF CELL AND DEVELOPMENTAL BIOLOGY*. 21:381-410.

Axelrod, D. 1981. Cell-substrate contacts illuminated by total internal-reflection fluorescence. *JOURNAL OF CELL BIOLOGY*. 89:141-145.

Axelrod, D. 2001. Total internal reflection fluorescence microscopy in cell biology. *TRAFFIC*. 2:764-774.

Berman, A., N. Kozova, and G. Morozevich. 2003. Integrins: Structure and signaling. *In* BIOCHEMISTRY-MOSCOW. Vol. 68. 1284-1299.

Bokoch, G., C. Vlahos, Y. Wang, U. Knaus, and A. TraynorKaplan. 1996. Rac GTPase interacts specifically with phosphatidylinositol 3-kinase. *BIOCHEMICAL JOURNAL*. 315:775-779.

Burridge, K., and K. Wennerberg. 2004. Rho and Rac take center stage. *CELL*. 116:167-179.

Cai, Y., N. Biais, G. Giannone, M. Tanase, G. Jiang, J. Hofman, C. Wiggins, P. Silberzan, A. Buguin, B. Ladoux, and M. Sheetz. 2006. Nonmuscle myosin IIA-dependent force inhibits cell spreading and drives F-actin flow. *BIOPHYSICAL JOURNAL*. 91:3907-3920.

Carragher, N., and M. Frame. 2004. Focal adhesion and actin dynamics: a place where kinases and proteases meet to promote invasion. *TRENDS IN CELL BIOLOGY*. 14:241-249.

Chen, H., P. Appeddu, H. Isoda, and J. Guan. 1996. Phosphorylation of tyrosine 397 in focal adhesion kinase is required for binding phosphatidylinositol 3-kinase. *JOURNAL OF BIOLOGICAL CHEMISTRY*. 271:26329-26334.

Chew, T., R. Masaracchia, Z. Goeckeler, and R. Wysolmerski. 1998. Phosphorylation of non-muscle myosin II regulatory light chain by p21-activated kinase (gamma-PAK). *JOURNAL OF MUSCLE RESEARCH AND CELL MOTILITY*. 19:839-854.

Clark, E.A., and J.S. Brugge. 1995. Integrins And Signal-Transduction Pathways - The Road Taken. *Science*. 268:233-239.

Craig, R., and J. Woodhead. 2006. Structure and function of myosin filaments. *CURRENT OPINION IN STRUCTURAL BIOLOGY*. 16:204-212.

Etienne-Manneville, S., and A. Hall. 2002. Rho GTPases in cell biology. *NATURE*. 420:629-635.

Gardiner, E., K. Pestonjamasp, B. Bohl, C. Chamberlain, K. Hahn, and G. Bokoch. 2002. Spatial and temporal analysis of Rac activation during live neutrophil chemotaxis. *CURRENT BIOLOGY*. 12:2029-2034.

Giancotti, F., and E. Ruoslahti. 1999. Transduction - Integrin signaling. *SCIENCE*. 285:1028-1032.

Gillespie, D. 1976. General method for numerically simulating stochastic time evolution of coupled chemical-reactions. *JOURNAL OF COMPUTATIONAL PHYSICS*. 22:403-434.

Guo, F., M. Debidda, L. Yang, D. Williams, and Y. Zheng. 2006. Genetic deletion of Rac1 GTPase reveals its critical role in actin stress fiber formation and focal adhesion complex assembly. *JOURNAL OF BIOLOGICAL CHEMISTRY*. 281:18652-18659.

Han, J., K. Luby-Phelps, B. Das, X. Shu, Y. Xia, R. Mosteller, U. Krishna, J. Falck, M. White, and D. Broek. 1998. Role of substrates and products of PI3-kinase in regulating activation of Rac-related guanosine triphosphatases by Vav. *SCIENCE*. 279:558-560.

Haslam, R., H. Koide, and B. Hemmings. 1993. Pleckstrin domain homology. *NATURE*. 363:309-310.

Haugh, J., F. Codazzi, M. Teruel, and T. Meyer. 2000. Spatial sensing in fibroblasts mediated by 3 ' phosphoinositides. *JOURNAL OF CELL BIOLOGY*. 151:1269-1279.

Heim, R., A. Cubitt, and R. Tsien. 1995. Improved green fluorescence. *NATURE*. 373:663-664.

Kiosses, W., R. Daniels, C. Otey, G. Bokoch, and M. Schwartz. 1999. A role for p21-activated kinase in endothelial cell migration. *JOURNAL OF CELL BIOLOGY*. 147:831-843.

Kolsch, V., P. Charest, and R. Firtel. 2008. The regulation of cell motility and chemotaxis by phospholipid signaling. *JOURNAL OF CELL SCIENCE*. 121:551-559.

Kraynov, V., C. Chamberlain, G. Bokoch, M. Schwartz, S. Slabaugh, and K. Hahn. 2000. Localized Rac activation dynamics visualized in living cells. *SCIENCE*. 290:333-337.

Leevers, S., B. Vanhaesebroeck, and M. Waterfield. 1999. Signalling through phosphoinositide 3-kinases: the lipids take centre stage. *CURRENT OPINION IN CELL BIOLOGY*. 11:219-225.

Lemmon, M., K. Ferguson, and C. Abrams. 2002. Pleckstrin homology domains and the cytoskeleton. *FEBS LETTERS*. 513:71-76.

Mitra, S., D. Hanson, and D. Schlaepfer. 2005. Focal adhesion kinase: In command and control of cell motility. *NATURE REVIEWS MOLECULAR CELL BIOLOGY*. 6:56-68.

Moissoglu, K., and M. Schwarz. 2006. Integrin signalling in directed cell migration. *BIOLOGY OF THE CELL*. 98:547-555.

Moissoglu, K., B. Slepchenko, N. Meller, A. Horwitz, and M. Schwartz. 2006. In vivo dynamics of Rac-membrane interactions. *MOLECULAR BIOLOGY OF THE CELL*. 17:2770-2779.

Nayal, A., D. Webb, C. Brown, E. Schaefer, M. Vicente-Manzanares, and A. Horwitz. 2006. Paxillin phosphorylation at ser273 localizes a GIT1-PIX-PAK complex and regulates adhesion and protrusion dynamics. *JOURNAL OF CELL BIOLOGY*. 173:587-599.

Nobes, C., and A. Hall. 1995. Rho, Rac, and Cdc42 GTPases regulate the assembly of multimolecular focal complexes associated with actin stress fibers, lamellipodia, and filopodia. *CELL*. 81:53-62.

Nobes, C., and A. Hall. 1999. Rho GTPases control polarity, protrusion, and adhesion during cell movement. *JOURNAL OF CELL BIOLOGY*. 144:1235-1244.

Pestonjamasp, K., C. Forster, C. Sun, E. Gardiner, B. Bohl, O. Weiner, G. Bokoch, and M. Glogauer. 2006. Rac1 links leading edge and uropod events through Rho and myosin activation during chemotaxis. *BLOOD*. 108:2814-2820.

Ridley, A., P. Comoglio, and A. Hall. 1995. Regulation of scatter factor hepatocyte growth-factor responses by Ras, Rac, and Rho in MDCK cells. *MOLECULAR AND CELLULAR BIOLOGY*. 15:1110-1122.

Ridley, A., and A. Hall. 1992. The small GTP-binding protein Rho regulates the assembly of focal adhesions and actin stress fibers in response to growth-factors. *CELL*. 70:389-399.

Ridley, A., H. Paterson, C. Johnston, D. Diekmann, and A. Hall. 1992. The small GTP-binding protein Rac regulates growth-factor induced membrane ruffling. *CELL*. 70:401-410.

Sanders, L., F. Matsumura, G. Bokoch, and P. de Lanerolle. 1999. Inhibition of myosin light chain kinase by p21-activated kinase. *SCIENCE*. 283:2083-2085.

Schaller, M. 2001. Paxillin: a focal adhesion-associated adaptor protein. *ONCOGENE*. 20:6459-6472.

Schwartz, M., M. Schaller, and M. Ginsberg. 1995. Integrins: Emerging paradigms of signal transduction. *ANNUAL REVIEW OF CELL AND DEVELOPMENTAL BIOLOGY*. 11:549-599.

Sellers, J., H. Goodson, and F. Wang. 1996. A myosin family reunion. *JOURNAL OF MUSCLE RESEARCH AND CELL MOTILITY*. 17:7-22.

Shaner, N., R. Campbell, P. Steinbach, B. Giepmans, A. Palmer, and R. Tsien. 2004. Improved monomeric red, orange and yellow fluorescent proteins derived from Discosoma sp red fluorescent protein. *NATURE BIOTECHNOLOGY*. 22:1567-1572.

Shoelson, S., M. Sivaraja, K. Williams, P. Hu, J. Schlessinger, and M. Weiss. 1993. Specific phosphopeptide binding regulates a conformational change in the PI 3-kinase SH2 domain associated with enzyme activation. *EMBO JOURNAL*. 12:795-802.

Tolias, K., L. Cantley, and C. Carpenter. 1995. Rho-family GTPases bind to phosphoinositide kinases. *JOURNAL OF BIOLOGICAL CHEMISTRY*. 270:17656-17659.

Vanhaesebroeck, B., S. Leevers, K. Ahmadi, J. Timms, R. Katso, P. Driscoll, R. Woscholski, P. Parker, and M. Waterfield. 2001. Synthesis and function of 3-phosphorylated inositol lipids. *ANNUAL REVIEW OF BIOCHEMISTRY*. 70:535-602.

Vanhaesebroeck, B., and M. Waterfield. 1999. Signaling by distinct classes of phosphoinositide 3-kinases. *EXPERIMENTAL CELL RESEARCH*. 253:239-254.

Vicente-Manzanares, M., J. Zareno, L. Whitmore, C. Choi, and A. Horwitz. 2007. Regulation of protrusion, adhesion dynamics, and polarity by myosins IIA and IIB in migrating cells. *JOURNAL OF CELL BIOLOGY*. 176:573-580.

Webb, D., K. Donais, L. Whitmore, S. Thomas, C. Turner, J. Parsons, and A. Horwitz. 2004. FAK-Src signalling through paxillin, ERK and MLCK regulates adhesion disassembly. *NATURE CELL BIOLOGY*. 6:154-161.

Welch, H., W. Coadwell, L. Stephens, and P. Hawkins. 2003. Phosphoinositide 3-kinase-dependent activation of Rac. *FEBS LETTERS*. 546:93-97.

Zamir, E., and B. Geiger. 2001. Molecular complexity and dynamics of cell-matrix adhesions. *JOURNAL OF CELL SCIENCE*. 114:3583-3590.

Zamir, E., M. Katz, Y. Posen, N. Erez, K. Yamada, B. Katz, S. Lin, D. Lin, A. Bershadsky, Z. Kam, and B. Geiger. 2000. Dynamics and segregation of cell-matrix adhesions in cultured fibroblasts. *NATURE CELL BIOLOGY*. 2:191-196.

CHAPTER 2: Integrin, PI3K and Rac signaling come together

2.1 INTRODUCTION

Cell migration is an important process for wound healing, embryonic development, and cancer metastasis. It involves protrusion and adhesion at the leading edge and retraction at the trailing end. The whole process involves a wide variety of structural and signaling proteins. Migrating cells receive and interpret signals from both soluble and adhesive external cues.

Different cell types respond to different soluble factors based on what receptor proteins they express on their surface. Platelet-derived growth factor (PDGF) is a potent chemoattractant for fibroblasts, because they express PDGF receptors in their membranes. The fibroblast response to PDGF is important for dermal wound healing, wherein cells in the wound secrete PDGF to recruit fibroblasts. Once fibroblasts are in the wound area, they secrete, remodel, and contract extracellular matrix (ECM) and thus close the wound. Activated PDGF receptors activate PI3K at the plasma membrane, which leads to production of PIP_3 lipids (Kundra et al., 1994). Downstream effectors of these lipids regulate various cellular responses.

Migrating cells are also regulated by immobilized stimuli. Fibronectin is a common ECM protein present in humans and serves as a docking site for integrin receptors. Upon binding to ECM, integrins cluster and recruit various proteins to form focal adhesion complexes. Focal adhesion kinase (FAK) is the key regulator in this complex and it interacts with PI3K (Zamir and Geiger, 2001).

Fibroblasts migrate also on artificial, positively charged surfaces such as poly-lysine. While migration on poly-lysine is less effective than on fibronectin, PI3K activity remains unchanged (Weiger, 2008). The mechanism of this activation is not fully understood.

Proteins with pleckstrin homology (PH) domains bind to PIP_3 at the membrane. Guanine exchange factors (GEFs) activate Rho family GTPases by catalyzing the

exchange of GDP for GTP, and PI3K activity effectively stimulates recruitment and activation of Rac at the membrane through PIP_3-mediated recruitment of Rac GEFs. Active, GTP-bound Rac stimulates protrusion in migrating cells, which results in more focal adhesions and therefore also more PI3K activity. Thus, if Rac and PI3K are co-localized in space and time, there is a potential for positive feedback.

In this Chapter, we present experiments with function-blocking anti-integrin antibodies, evaluating their effects on spreading of fibroblasts on both fibronectin and poly-lysine. We show that spreading on fibronectin is largely inhibited by this antibody but does not affect PI3K signaling on poly-lysine. We show the spatial and temporal distribution of Rac and PI3K during random migration and during addition of a saturating concentration of PDGF.

2.2 MATERIALS AND METHODS

2.2.1 Cell culture and reagents

Spreading experiments with anti-β_1 integrin antibodies were performed with NIH 3T3 mouse fibroblasts (American Type Culture Collection) in which the PIP_3-specific biosensor construct EGFP-AktPH (Haugh et al., 2000) was stably expressed. The EGFP-AktPH construct was cloned into the NotI and BamHI sites of the pBM-IRES-Puro retroviral vector (a gift from Dr. Steven Wiley and Dr. Lee Opresko, Pacific Northwest National Laboratory). This vector was transfected into the ecotropic ϕNX viral packaging cell line by the calcium precipitation method, and the viral supernatants were used for infection of NIH 3T3 fibroblasts (Kaur et al., 2006). After infection, cells were cultured in regular growth medium (Dulbecco's modified Eagle's medium supplemented with 10% fetal bovine serum and 1% penicillin/streptomycin/glutamate) and further selected with 2-4 μg/ml of puromycin. All tissue culture reagents were purchased from Invitrogen (Carlsbad, CA). All imaging experiments were performed using cells between passages 10-30.

In long-term migration experiments, NIH 3T3 cells were transiently transfected with EGFP-wtRac1 (wild-type; a gift from Dr. Martin Schwartz, University of Virginia) and

mCherry-AktPH constructs using Lipofectamine Plus reagent (Invitrogen). The wild-type Rac1 gene was cloned into pEGFP-C1 to make the EGFP-wtRac1 construct (del Pozo et al., 1999). The mCherry-AktPH construct was cloned by replacing EGFP in C1-EGFP-AktPH with the mCherry gene (a gift from Dr. Roger Tsien, University of California, San Diego) using AgeI and BglII restriction sites. Transfected cells were observed by TIRF microscopy 24-36hr post transfection.

Human plasma fibronectin and anti-β_1 integrin antibodies (hamster anti-rat CD29) were obtained from BD Biosciences (San Jose, CA) and Invitrogen and BD Pharmingen, respectively. Human recombinant PDGF-BB was from Peprotech (Rocky Hill NJ). PI3K inhibitors LY294002 and wortmannin were from Calbiochem (San Diego, CA) and Sigma (St. Louis, MO), respectively.

2.2.2 Cell spreading experiments with β_1-integrin antibody

For spreading experiments, EGFP-AktPH-expressing cells were serum-starved for 2.5 hours and then detached with a brief trypsin-EDTA treatment and suspended in imaging buffer (20 mM HEPES pH 7.4, 125 mM NaCl, 5 mM KCl, 1.5 mM $MgCl_2$, 1.5 mM $CaCl_2$, 10 mM glucose, and 2 mg/ml fatty acid-free bovine serum albumin). After centrifugation at 100xg for 3 min, the cells were re-suspended in imaging buffer and 20 μg/ml of β_1-integrin antibody was added. Cells were incubated in suspension at a density of 10^4 cells/ml in the presence of the antibody for 30 min at 37°C prior to imaging. Adhesive surfaces were prepared on clean, sterile glass cover slips, which were coated with poly-D-lysine (100 μg/ml) for 2 h at room temperature or fibronectin (10 μg/ml) for 1 h at 37°C, washed with deionized, sterile water, and dried within 30 min of the experiment.

2.2.3 Long term migration experiments

NIH 3T3 cell transiently transfected with EGFP-wtRac1 and mCherry-AktPH were used for long term migration experiments. Cells were detached with a brief trypsin-EDTA treatment and suspended in imaging supplemented with 1% fetal bovine serum (FBS) (Gibco/Invitrogen). After centrifugation at 100xg for 3 min, 10,000 cells were

resuspended in 1 ml of imaging buffer and allowed to spread onto fibronectin (10 μg/ml) coated cover slips for 2 h. Once attached, cells were observed by TIRF microscopy at 37°C. To prevent evaporation, 200 μl of mineral oil (Sigma) was added to cover the imaging buffer.

2.2.4 Phase contrast microscopy

Phase contrast microscopy was used to investigate the effect of β_1-integrin antibody on spreading. A Zeiss Axiovert 25 inverted microscope with LD A-Plan 20X (0.3 NA) objective was used to observe the cells. Digital images were taken with a Canon Powershot G5 digital camera at specified time points. Cells were incubated at 37°C and 5% CO_2 between image acquisitions.

2.2.5 TIRF microscopy

TIRF microscopy is used to selectively excite fluorophores within ~ 100 nm of the glass-buffer interface, which effectively illuminates the plasma membrane contact area (Schneider and Haugh, 2004).

Our prism-based TIRF microscope has been described in detail previously (Schneider et al., 2005). EGFP was excited using a 60 mW 488 nm line from a tunable wavelength argon ion laser head (Melles Griot, Irvine, CA). The red fluorescent protein mCherry was excited by a 100 mW diode-pumped 561 nm line (Crystalaser, Reno, NV). A 20X water immersion objective (Zeiss Achroplan, 0.5 NA) and 0.63X camera mount were used. Digital images, with 2x2 binning, were acquired at regular intervals (15 s for spreading experiments and 2 min for migration experiments) using a Hamamatsu ORCA ER cooled CCD (Hamamatsu, Bridgewater, NJ). The exposure time was 600 ms and gain of 2 unless otherwise stated. Digital images were acquired and processed using Metamorph software (Universal Imaging, West Chester, PA). A custom-built temperature control chamber was used to maintain a temperature of ~ 37°C.

2.3 RESULTS

2.3.1 β_1-integrin antibody inhibits spreading on fibronectin but has no effect on spreading or PI3K signaling on poly-lysine

Fibroblasts spread effectively on both fibronectin and poly-lysine. Adhesion on fibronectin is mediated by integrins (Clark and Brugge, 1995). In the case of poly-lysine, the mechanism of adhesion is thought to be through non-specific, electrostatic interactions, but the possibility of its activating integrins or other specific cell surface receptors has not been fully addressed. To assess the role of integrins during spreading we incubated stable expressing EGFP-AktPH NIH 3T3 mouse fibroblasts with β_1-integrin antibodies (20 μg/ml) before spreading on fibronectin and poly-lysine coated glass cover slips.

Spreading on fibronectin in the presence of antibody was strongly inhibited, resulting in a smaller number of attached cells and lack of fully spread cell phenotype (Figure 2.1). By comparison, the antibody has a minimal effect on spreading on poly-lysine, which normally occurs with slower kinetics. Cells were allowed to spread in imaging buffer at 37°C and 5% CO_2. Phase microscopy images shown in Figure 2.1 were acquired 90 minutes after addition of cells and the same number of cells (10^4) was added to each cover slip.

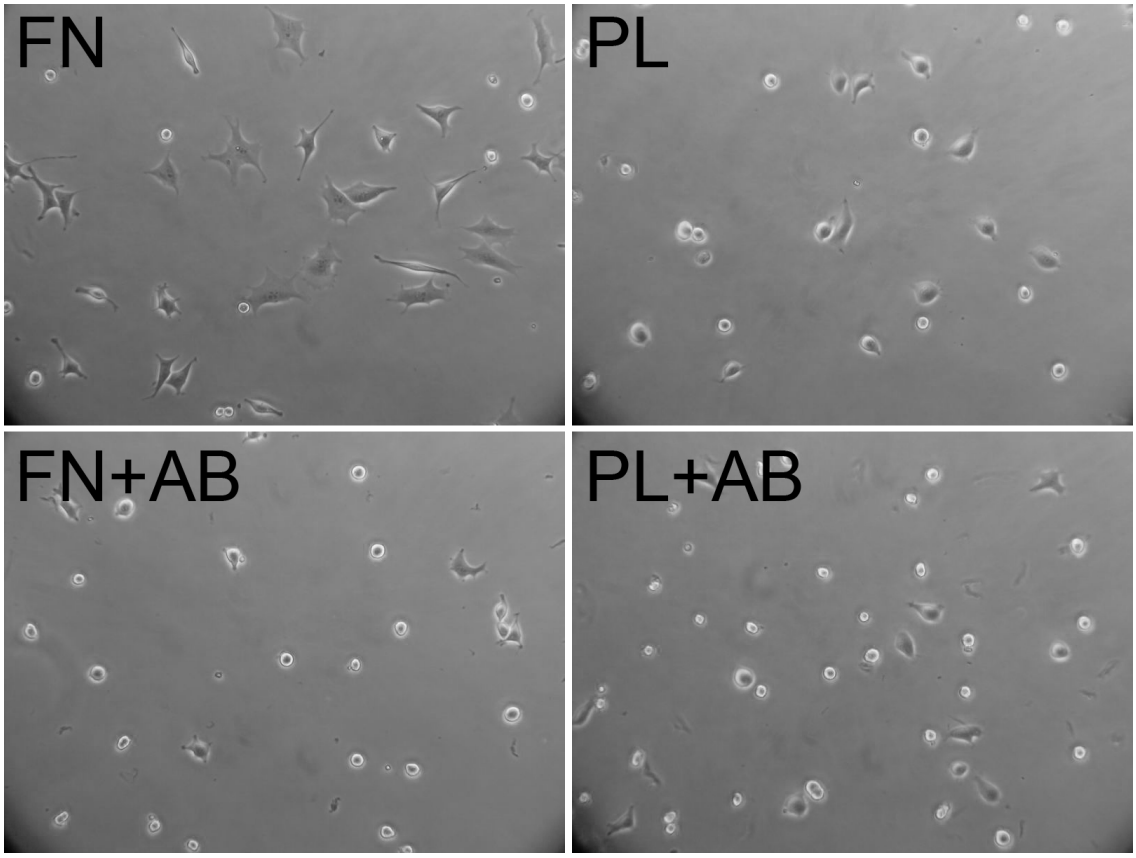

Figure 2.1 Effects of β_1-integrin antibody on fibroblast spreading. Mouse NIH 3T3 fibroblasts with stable expression of EGFP-AktPH were incubated for 30 minutes in the presence of anti- β_1 integrin antibody (AB) or in control buffer. After antibody treatment, cells were allowed to spread on fibronectin (FN) or poly-lysine (PL) coated surfaces for 90 minutes. Adhesion of cells on fibronectin is significantly reduced in the presence of the antibody. The antibody has no discernible effect on adhesion on poly-lysine.

To partially assess the mechanism of PI3K activation during spreading, we monitored with TIRF microscopy spreading of stably expressing EGFP-AktPH cells in the presence of β_1-integrin antibody. After serum starvation, cells were detached and suspended for 30 minutes in extracellular buffer with the antibody (20 μg/ml). After incubation, 10^4 cells were added to poly-lysine coated glass cover slips. The images in Figure 2.2 show representative cells at specified times after cell addition. After 40 minutes, cells were uniformly stimulated with 5 nM PDGF to elicit maximum PI3K activity. At 50 minutes, cells were uniformly inhibited with 5 μM wortmannin to rapidly abolish PI3K activity.

As shown in Figure 2.2, there is no discernible difference in PI3K activity during spreading on poly-lysine between control cells and cells incubated with β_1-integrin antibody. PI3K is spontaneously activated during spreading on poly-lysine. Saturating PDGF stimulation causes high localization of PI3K activity at the cell periphery, whereas the intensity level attributed to cytosolic fluorescence is revealed by the high dose of wortmannin.

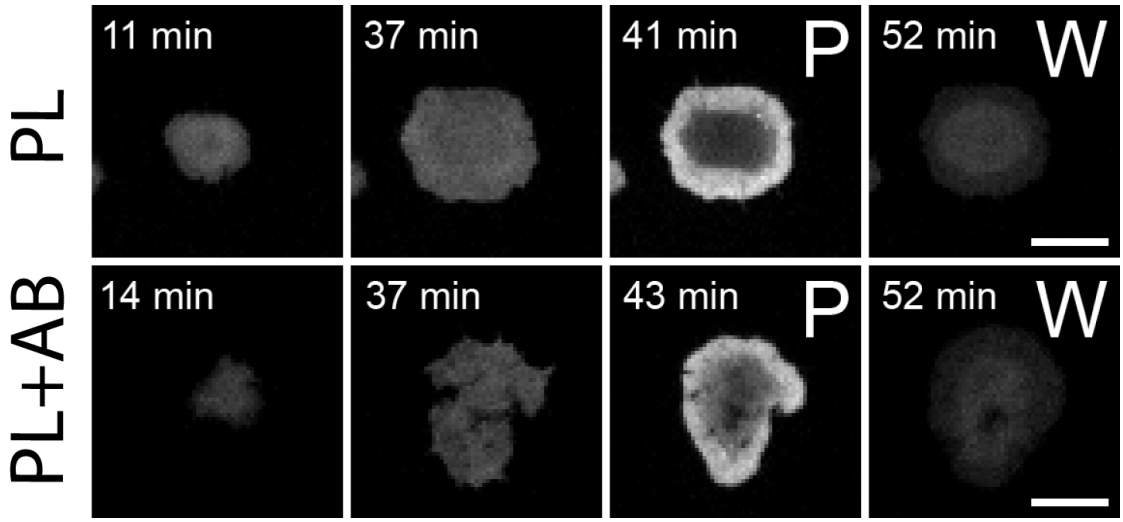

Figure 2.2 PI3K activity during fibroblast spreading on poly-lysine in the presence of β_1-integrin antibody. EGFP-AktPH-expressing NIH3T3 mouse fibroblasts incubated with β_1-integrin antibody (20 μg/mL) were imaged by TIRF microscopy during spreading on poly-lysine coated glass cover slips. Images were acquired at the indicated times after addition of cells. Control cell spreading on poly-lysine (PL) is shown in the top row and cell after antibody incubation (PL+AB) is shown in the bottom row. Maximal concentrations of PDGF (P) (5 nM) and wortmannin (W) (5 μM) were added to stimulate and inhibit PI3K activity, respectively. The β_1-integrin antibody has no detectable influence on PI3K activity during spreading on poly-lysine. Scale bars = 20 μm.

2.3.2 Stimulation of PI3K activity with PDGF has a minimal effect on Rac activity

To examine the spatial co-localization of PI3K and Rac, we transiently transfected NIH 3T3 mouse fibroblasts with EGFP-Rac and mCherry-AktPH. The cells were plated on fibronectin-coated glass cover slips and allowed to attach. After 2.5 hour serum starvation, the cells were imaged by TIRF microscopy. In Figure 2.3 we show the fluorescence pattern of each biosensor in the basal state and 1 minute and 9 minutes post-stimulation with 5 nM PDGF. PI3K activity is rapidly distributed to the cell periphery after PDGF stimulation, while there is no discernible change in EGFP-Rac translocation.

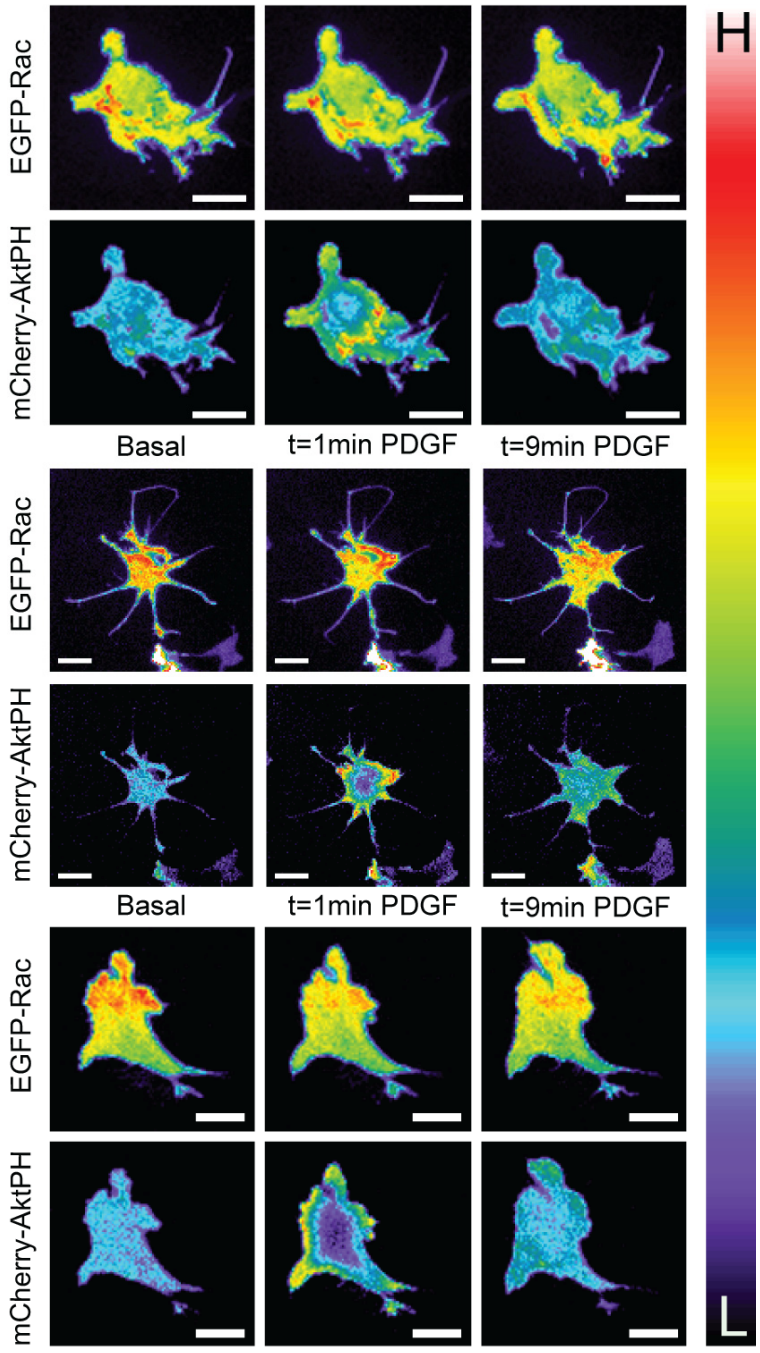

Figure 2.3 PI3K and Rac activity during PDGF stimulation. NIH 3T3 mouse fibroblasts transiently transfected with EGFP-Rac1 and mCherry-AktPH were plated on fibronectin coated glass cover slips. After 2.5 hour serum starvation, cells were observed by TIRF microscopy. Cells are shown at basal state, 1 minute and 9 minutes after 5 nM PDGF stimulation. PI3K activity is efficiently translocated to the cell periphery after PDGF stimulation, but no significant change in Rac distribution was detected. Pseudocolor scale is shown on the right with highest (H) and lowest (L) levels indicated. Scale bars = 20 μm.

2.3.3 PI3K and Rac are co-localized during random migration

Migration is a cyclic process of membrane protrusion and adhesion at the leading edge followed by retraction at the trailing edge. Active Rac promotes lamellipodia formation at the leading edge, and PI3K is involved in directed migration during wound healing. To investigate the spatial distribution of Rac and PI3K during migration, we transiently transfected NIH 3T3 fibroblasts with EGFP-Rac1 and mCherry-AktPH. Cells were plated on fibronectin-coated cover slips and allowed to attach for 2.5 hours in imaging buffer supplemented with 1% FBS. Cells were allowed to migrate for 4 hours, and then PI3K was maximally inhibited with 100 μM LY294002. Rac and PI3K were co-localized the majority of the time in protruding areas of the cell (Fig. 2.4). As with PI3K stimulation by PDGF, inhibition of PI3K activity had minimal effect on Rac localization.

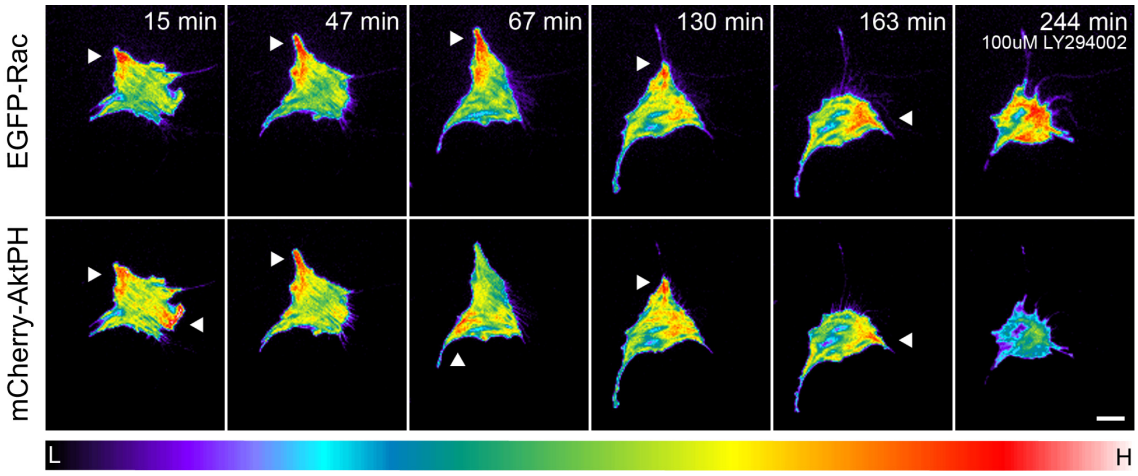

Figure 2.4 Co-localization of PI3K and Rac in fibroblasts during random migration. NIH 3T3 mouse fibroblasts transiently transfected with EGFP-Rac1 and mCherry-AktPH were plated on fibronectin-coated glass cover slips in imaging buffer with 1% FBS. Cells were allowed to migrate for 4 hours at 37°C and then uniformly inhibited with 100 μM LY294002. Pseudocolor TIRF images are shown at specified time points with arrows pointing to areas of high activity. Pseudocolor scale is shown on the bottom with lowest (L) and highest (H) levels indicated. Scale bars = 20 μm.

2.4 DISCUSSION

Mouse fibroblasts spread effectively on both fibronectin and poly-lysine coated glass cover slips. Integrins bind the RGD sequence of fibronectin and mediate adhesion and intracellular signaling. In the case of poly-lysine, it is believed that the initial attraction force is between negatively charge plasma membrane and positively charged poly-lysine. Previous work in our laboratory has revealed that PI3K, a major mediator of cell motility, is activated to a similar degree on both surfaces (Weiger, 2008). To further assess the role of integrins during cell spreading we incubated cells with β_1-integrin antibodies and allowed them to spread on both surfaces. Adhesion on fibronectin was significantly impaired, but minimal change was observed on poly-lysine (Fig. 2.1), indicating that the surfaces elicit adhesion by different mechanisms. Although we cannot completely rule out the possibility that integrins other than those that engage fibronectin are being activated on poly-lysine, other evidence obtained by our group has shown that phosphorylation of FAK and paxillin, which are classical integrin-mediated signaling readouts, are detectable on fibronectin but not poly-lysine (Weiger, 2008).

PI3K is activated in response to integrin-mediated adhesion to ECM. In cells spreading on poly-lysine, PI3K is activated to a similar extent as in the case of fibronectin (Weiger, 2008). We observed PI3K activity in cells spreading on poly-lysine after β_1-integrin antibody incubation. The antibody had no discernible effect on PI3K activity during spreading on poly-lysine (Fig. 2.2). The activation of PI3K on charged surfaces is not understood, but we propose two different possibilities. First, a receptor other than integrins may be activated resulting in PI3K activity. Another possibility is that PI3K signaling responds to mechanical stimulation that results from attachment to a rigid surface.

The small GTPase Rac is an important regulator of cell migration. In its active state, Rac stimulates formation of lamellipodia. PI3K promotes recruitment of GEFs that stimulate Rac activation, and Rac partially increases PI3K activity, suggesting a feedback loop (Bokoch et al., 1996; Han et al., 1998; Welch et al., 2003). Using TIRF

microscopy, we studied cells expressing both EGFP-Rac and mCherry-AktPH. Stimulation of PI3K activity by PGDF has a minimal effect on Rac activity in quiescent cells (Fig. 2.3). We conclude that PI3K is not a master regulator of Rac activity and recommend that their interaction needs to be studied under conditions where PI3K activity is not saturated, when more subtle effects might be observed.

During random migration, PI3K and Rac are often, but not always, co-localized at the leading protrusions (Fig. 2.4). This reinforces the observation from Fig. 2.3 that Rac is not a major target of PI3K-dependent signaling pathways. However, Rac and PI3K are often active in the same subcellular locations, suggesting some interplay between the two. The role of PI3K as a sole mediator of chemotaxis has been contested and at least four key signaling pathways are involved (Veltman et al., 2008). It is possible that PI3K and Rac influence cell motility by parallel or/and common pathways.

2.5 REFERENCES

Bokoch, G., C. Vlahos, Y. Wang, U. Knaus, and A. TraynorKaplan. 1996. Rac GTPase interacts specifically with phosphatidylinositol 3-kinase. *BIOCHEMICAL JOURNAL*. 315:775-779.

Clark, E.A., and J.S. Brugge. 1995. Integrins And Signal-Transduction Pathways - The Road Taken. *Science*. 268:233-239.

del Pozo, M., M. Vicente-Manzanares, R. Tejedor, J. Serrador, and F. Sanchez-Madrid. 1999. Rho GTPases control migration and polarization of adhesion molecules and cytoskeletal ERM components in T lymphocytes. *EUROPEAN JOURNAL OF IMMUNOLOGY*. 29:3609-3620.

Han, J., K. Luby-Phelps, B. Das, X. Shu, Y. Xia, R. Mosteller, U. Krishna, J. Falck, M. White, and D. Broek. 1998. Role of substrates and products of PI3-kinase in regulating activation of Rac-related guanosine triphosphatases by Vav. *SCIENCE*. 279:558-560.

Haugh, J., F. Codazzi, M. Teruel, and T. Meyer. 2000. Spatial sensing in fibroblasts mediated by 3 ' phosphoinositides. *JOURNAL OF CELL BIOLOGY*. 151:1269-1279.

Kaur, H., C. Park, J. Lewis, and J. Haugh. 2006. Quantitative model of Ras-phosphoinositide 3-kinase signalling cross-talk based on co-operative molecular assembly. *BIOCHEMICAL JOURNAL*. 393:235-243.

Kundra, V., J. Escobedo, A. Kazlauskas, H. Kim, S. Rhee, L. Williams, and B. Zetter. 1994. Regulation of chemotaxis by the platelet-derived growth-factor receptor-beta. *NATURE*. 367:474-476.

Schneider, I., and J. Haugh. 2004. Spatial analysis of 3 ' phosphoinositide signaling in living fibroblasts: II. Parameter estimates for individual cells from experiments. *BIOPHYSICAL JOURNAL*. 86:599-608.

Schneider, I., E. Parrish, and J. Haugh. 2005. Spatial analysis of 3 ' phosphoinositide signaling in living fibroblasts, III: Influence of cell morphology and morphological polarity. *BIOPHYSICAL JOURNAL*. 89:1420-1430.

Veltman, D., I. Keizer-Gunnik, and P. Van Haastert. 2008. Four key signaling pathways mediating chemotaxis in Dictyostelium discoideum. *JOURNAL OF CELL BIOLOGY*. 180:747-753.

Weiger, M. 2008. Integration of Soluble and Adhesive Signals during Fibroblast Migration. *In* Chemical Engineering. Vol. PhD. North Carolina State University, Raleigh, NC. 143.

Welch, H., W. Coadwell, L. Stephens, and P. Hawkins. 2003. Phosphoinositide 3-kinase-dependent activation of Rac. *FEBS LETTERS*. 546:93-97.

Zamir, E., and B. Geiger. 2001. Molecular complexity and dynamics of cell-matrix adhesions. *JOURNAL OF CELL SCIENCE*. 114:3583-3590.

CHAPTER 3: Signaling at the leading edge

3.1 INTRODUCTION

The mechanisms governing the formation and disassembly of integrin-extracellular matrix (ECM) adhesion complexes at the protruding leading edge are central to the understanding of cell migration. Active Rac promotes protrusion, accompanied by the formation of nascent focal adhesions (Pestonjamasp et al., 2006). Nascent adhesions either disassemble (turn over) or mature into stable focal adhesions. These two types of adhesion complexes are easily distinguished by total internal reflection fluorescence (TIRF) microscopy of EGFP-paxillin-expressing cells. Activation of Pak (p21-activated kinase) is mediated by nascent adhesions through a positive feedback involving phosphorylation of paxillin Ser273 by Pak and recruitment of Git1-βPix-Pak complexes, which in turn mediate activation of Rac and Pak (Nayal et al., 2006). Pak activity promotes turnover of nascent adhesions locally, whereas maturation of nascent adhesions is promoted in a more global fashion by actomyosin-mediated contractility (Vicente-Manzanares et al., 2007).

It is well known that the speed of cell migration depends on the ECM density. Cells tend to migrate fastest at intermediate levels of integrin-ECM engagement (Palecek et al., 1997). The tradeoff between low vs. high adhesion strength has been modeled successfully in physical terms as a compromise between cell traction and "static friction" with the underlying substratum (DiMilla et al., 1991). Recently, this tradeoff has been cast in terms of the coupling between adhesion and protrusion (Gupton and Waterman-Storer, 2006), but the distinction between nascent vs. stable adhesions and the specific roles of signal transduction processes in this coupling remain unclear.

We have developed a simplified mathematical model that incorporates adhesion and protrusion dynamics mediated by Rac/Pak signaling at the leading edge. The core of the model is the action of Pak in the aforementioned feedback loop that simultaneously promotes cell protrusion and turnover of nascent adhesions. The mechanisms that

negatively regulate this protrusion signaling are currently not well understood, and so our model allows for three speculative possibilities:

1. Stable adhesions promote further maturation of adhesions by globally enhancing the activity/recruitment of actomyosin.
2. Stable adhesions locally or globally antagonize Rac, perhaps via Rho signaling, conceptualized in the model as activation of a diffusible GTPase-accelerating protein (GAP).
3. Stable adhesions locally inhibit protrusion at the level of fluid/membrane mechanics.

Our goal is to relate the model to experimental observations in order to elucidate the coupling between signaling, protrusion, and adhesion dynamics at the microscopic scale, and the control of cell migration persistence at the macroscopic scale, both in the context of normal cell migration and perturbations of Rac/Pak signaling.

3.2 MODEL FORMULATION

3.2.1 Formation and maturation of adhesions

We define a hypothetical species called protrusive actin (*P.actin*) that is rapidly generated spontaneously and also in response to activated Rac (Rac*). Stable adhesions (*SA*) are thought to inhibit this process locally by a mechanical and/or signaling mechanism (if not, $K_{inhibit}$ is simply set to zero). For all species, square brackets signify local densities or concentrations.

$$[P.actin] = \frac{K_0 + K_{PA}[Rac^*]}{1 + K_{inhibit}[SA]} \tag{3.1}$$

Nascent adhesions (*NA*) assemble in response to the presence of protrusive actin, the rationale being that protrusion is a mechanism for exploring new regions of the substratum and for convective transport of unbound integrins from the top of the cell. This relationship is also a positive function of the extracellular matrix (ECM) density.

Nascent adhesions turn over or mature to form stable adhesions. Turnover responds locally to the activity of Pak associated with nascent adhesions (*Pak**; see below). Maturation is an increasing function of contraction force, stimulated globally by the stable adhesions, which mediate actomyosin activity (*Myo**) in a centralized region of the cell. At least in the mathematical context, the global nature of this regulation mechanism is achieved by allowing *Myo** to diffuse, at a potentially rapid rate. Alternatively, if contractility does not affect maturation of adhesions, the proportionality constant $K_{contract}$ is simply set to zero. Finally, stable adhesions are assumed to disassemble spontaneously.

$$\begin{aligned}\frac{d[NA]}{dt} &= k_{a,NA}^{ECM}[P.actin] \\ &\quad -k_{d,NA}\left(1+K_{turnover}[Pak^*]\right)[NA] \\ &\quad -k_{mature}\left(1+K_{contract}[Myo^*]\right)[NA];\end{aligned} \tag{3.2}$$

$$\begin{aligned}\frac{d[SA]}{dt} &= k_{mature}\left(1+K_{contract}[Myo^*]\right)[NA] \\ &\quad -k_{d,SA}[SA].\end{aligned} \tag{3.3}$$

$$\begin{aligned}\frac{\partial[Myo^*]}{\partial t} &= D_{Myo}\nabla^2[Myo^*] \\ &\quad +k_{a,Myo}[SA]-k_{d,Myo}[Myo^*].\end{aligned} \tag{3.4}$$

The superscript in the parameter $k_{a,NA}^{ECM}$ signifies that it depends in a positive way on the density and composition of the ECM.

3.2.2 Activation of a paxillin/Rac/Pak feedback loop by nascent adhesions

Paxillin is assumed to be abundant in the cytosol, and so bound paxillin is considered to be proportional to the number of nascent adhesions. Hence, the variable *NA* implies nascent adhesions bound with paxillin. Paxillin has numerous phosphorylation sites, but phosphorylated paxillin is taken here to mean paxillin capable of recruiting GIT1/βPix/Pak complexes. Nascent adhesions bound to phosphorylated paxillin ($NA \cdot Pax^*$) are generated in a manner that depends on the local Pak activity (*Pak**). There is also a small basal phosphorylation rate, the rationale being a mathematical one: it allows $[NA \cdot Pax^*]$ to evolve in time when its initial value is zero.

These adhesions, constituting a fraction of the total NA, are also subject to the same turnover mechanism as in Eq. 3.2, but it is considered to be slow compared to the phosphorylation/dephosphorylation kinetics.

$$\frac{d[NA \cdot Pax^*]}{dt} = k_{a,Pax}\left(Pak_0 + [Pak^*]\right)\left([NA] - [NA \cdot Pax^*]\right) - k_{d,Pax}[NA \cdot Pax^*] \quad \text{(fast)}. \tag{3.5}$$

Nascent adhesions in complex with phosphorylated paxillin mediate Rac activation through the GEF activity of βPix; βPix recruitment is implicit in the model. Active Rac is allowed to be mobile, modeled as a diffusive process, and Rac is deactivated by GTPase-accelerating proteins, which we allow to be activated by stable adhesions (possibly through Rho signaling); we introduce the species *GAP** to represent this regulation mechanism, the localization of which is controlled by a diffusive process.

$$\frac{\partial[Rac^*]}{\partial t} = D_{Rac}\nabla^2[Rac^*] + k_{a,Rac}[NA \cdot Pax^*] - k_{d,Rac}\left(1 + K_{GAP}[GAP^*]\right)[Rac^*]. \tag{3.6}$$

$$\frac{\partial[GAP^*]}{\partial t} = D_{GAP}\nabla^2[GAP^*] + k_{a,GAP}[SA] - k_{d,GAP}[GAP^*]. \tag{3.7}$$

A more global regulation is achieved by a assigning a large value for the diffusion coefficient, D_{GAP}. Setting $K_{GAP} = 0$ negates the mechanism altogether.

Pak is activated when nascent adhesions in complex with phosphorylated paxillin, which coordinate Pak recruitment, encounter active Rac. As in Eq. 3.5, the rate of turnover of these adhesions is neglected compared to the rates of activation/deactivation.

$$\frac{d[NA \cdot Pak^*]}{dt} = k_{a,Pak}\left([NA \cdot Pax^*] - [NA \cdot Pak^*]\right)[Rac^*] - k_{d,Pak}[NA \cdot Pak^*] \quad \text{(fast)}. \tag{3.8}$$

Finally, the local Pak activity, $[Pak^*]$ is taken to be proportional to $[NA \cdot Pak^*]$, and because $[Pak^*]$ has arbitrary units, we find it convenient to simply equate the two: $[NA \cdot Pak^*] \rightarrow [Pak^*]$. A schematic of the entire model is shown in Figure 3.1.

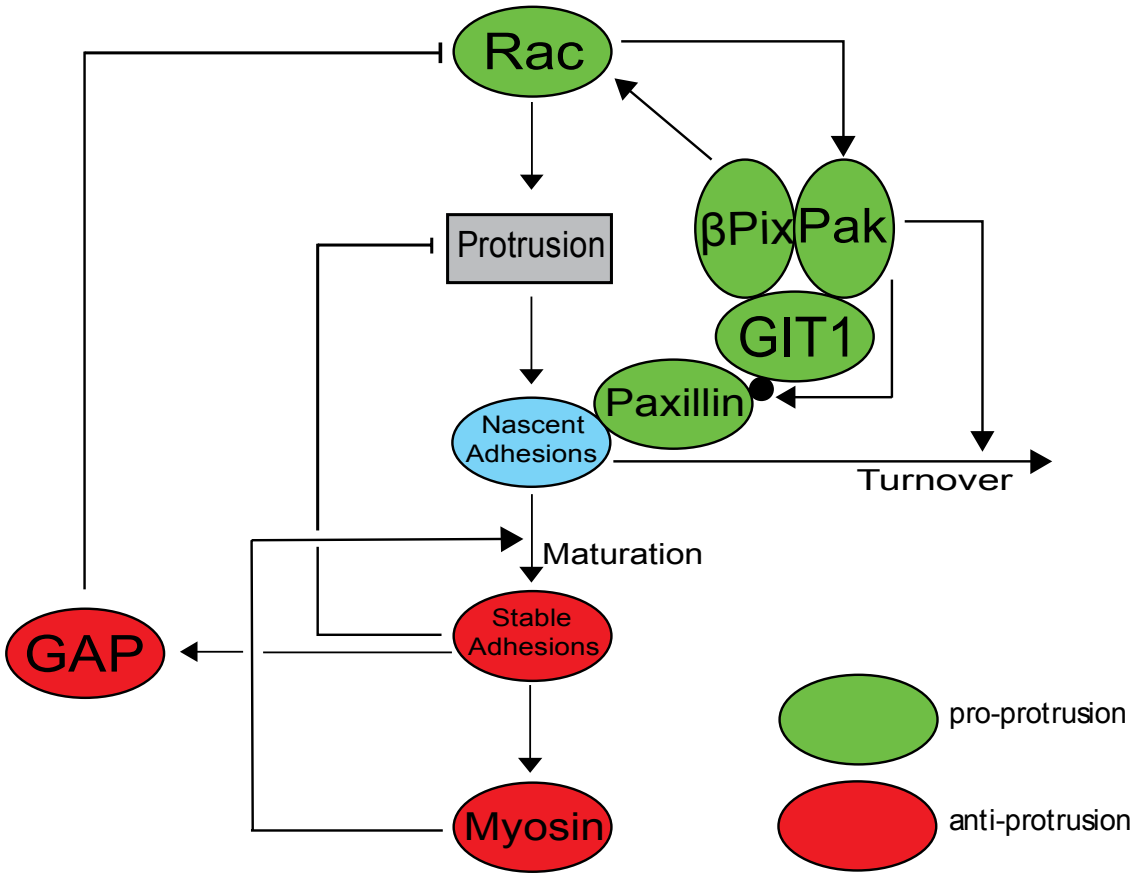

Figure 3.1 Model Schematic

3.2.3 Dimensionless model equations and parameters

The model outlined in Eqs. 3.1-3.8 is reduced to a dimensionless form as follows:

$$\frac{dn}{dt} = k_{d,NA}\left\{ G_n^{ECM}\left(\frac{1+E_n r}{1+I_n s}\right) - \left[1+p+C_n\left(1+E_s m\right)\right]n \right\} \qquad (3.9)$$

$$\frac{ds}{dt} = k_{d,SA}\left[\left(1+E_s m\right)n - s\right] \qquad (3.10)$$

$$\frac{\partial m}{\partial t} = k_{d,Myo}\left(L_m{}^2\nabla^2 m + s - m\right) \qquad (3.11)$$

$$\frac{dx}{dt} = k_{d,Pax}\left[G_x\left(P_0+p\right)\left(n-x\right) - x\right] \quad \text{(fast)} \qquad (3.12)$$

$$\frac{\partial r}{\partial t} = k_{d,Rac}\left[L_r{}^2\nabla^2 r + x - (1 + C_r g)r\right] \tag{3.13}$$

$$\frac{\partial g}{\partial t} = k_{d,GAP}\left[L_g{}^2\nabla^2 g + s - g\right] \tag{3.14}$$

$$\frac{dp}{dt} = k_{d,Pak}\left[r(x - K_p p) - p\right] \quad \text{(fast)} \tag{3.15}$$

The dimensionless variables are denoted by lowercase letters, defined as follows:

$$n = \frac{[NA]}{NA^\dagger} \tag{3.16}$$

$$s = \frac{k_{d,SA}}{k_{mature}}\frac{[SA]}{NA^\dagger} \tag{3.17}$$

$$m = \frac{k_{d,Myo}}{k_{a,Myo}}\frac{k_{d,SA}}{k_{mature}}\frac{[Myo^*]}{NA^\dagger} \tag{3.18}$$

$$x = \frac{[NA \cdot Pax^*]}{NA^\dagger} \tag{3.19}$$

$$r = \frac{k_{d,Rac}}{k_{a,Rac}}\frac{[Rac^*]}{NA^\dagger} \tag{3.20}$$

$$g = \frac{k_{d,GAP}}{k_{a,GAP}}\frac{k_{d,SA}}{k_{mature}}\frac{[GAP^*]}{NA^\dagger} \tag{3.21}$$

$$p = K_{turnover}[Pak^*] \tag{3.22}$$

$$NA^\dagger = \left(\frac{k_{d,Pax}k_{d,Rac}k_{d,Pak}}{k_{a,Pax}k_{a,Rac}k_{a,Pak}}\right)^{1/2} \tag{3.23}$$

The dimensionless parameters of the model are denoted by capital letters with subscripts. Parameters are classified as to whether they characterize generation or growth (G_n^{ECM}, G_x), consumption (C_n, C_r), enhancement (E_n, E_s), or inhibition (I_n) processes. Two others refer to diffusion length scales, relative to a unit domain size (L_m, L_g), and the two remaining parameters characterize the basal Pak activity (P_0) and saturation of Rac-mediated Pak activation (K_p).

$$G_n^{ECM} = \frac{K_0}{NA^\dagger}\frac{k_{a,NA}^{ECM}}{k_{d,NA}} \tag{3.24}$$

$$G_x = \frac{k_{a,Pax}}{k_{d,Pax}K_{turnover}} \tag{3.25}$$

$$E_n = \frac{K_{PA}}{K_0}\frac{k_{a,Rac}}{k_{d,Rac}}NA^\dagger \tag{3.26}$$

$$E_s = K_{contract}\frac{k_{a,Myo}}{k_{d,Myo}}NA^\dagger \tag{3.27}$$

$$C_n = \frac{k_{mature}}{k_{d,NA}} \tag{3.28}$$

$$C_r = K_{GAP}\frac{k_{a,GAP}}{k_{d,GAP}}\frac{k_{mature}}{k_{d,SA}}NA^\dagger \tag{3.29}$$

$$I_n = K_{inhibit}\frac{k_{mature}}{k_{d,SA}}NA^\dagger \tag{3.30}$$

$$K_p = \frac{k_{a,Pak}}{k_{d,Pak}}\frac{k_{a,Rac}}{k_{d,Rac}}NA^\dagger \tag{3.31}$$

$$P_0 = K_{turnover}Pak_0 \tag{3.32}$$

$$L_m = \left(\frac{D_{Myo}}{k_{d,Myo}}\right)^{1/2} \tag{3.33}$$

$$L_r = \left(\frac{D_{Rac}}{k_{d,Rac}}\right)^{1/2} \tag{3.34}$$

$$L_g = \left(\frac{D_{GAP}}{k_{d,GAP}}\right)^{1/2} \tag{3.35}$$

The model is scaled so that the triggering of the paxillin/Rac/Pak feedback loop is significant when x, r, and p are ~ 1 or greater. Hence, certain parameter values are assigned as follows.

1. Protrusion responds robustly to Rac signaling ($E_n >> 1$); $E_n = 10$.
2. Pak activity in the absence of adhesion should be low ($P_0 << 1$); $P_0 = 0.01$.
3. When $x \sim 1$, Pak should not be saturated by Rac ($K_p << 1$); $K_p = 0.1$.
4. When adhesion strength is low, most NAs turn over rather than mature ($C_n << 1$); $C_n = 0.1$.

The parameter G_n^{ECM} is varied to affect changes in ECM density, and the remaining parameters were varied systematically. The parameter G_x compares Pak's influence on paxillin phosphorylation relative to its influence on NA turnover; values between 0.1 and 10 are to be explored, with $G_x = 1$ taken as the base value. The parameters I_n, E_s, and C_r quantify the possible effects of stable adhesions on inhibition of protrusion (local), actomyosin-mediated adhesion maturation (local or global, depending on whether L_m is << 1 or ~ 1 or larger) and activation of Rac-GAP (local or global, depending on whether L_g is << 1 or ~ 1 or larger), respectively. As outlined above, any of these effects is silenced by setting its parameter to zero. Default parameter values are shown in Table 3.1.

Table 3.1 Values of dimensionless parameters. Default values are shown bold.

Parameter	Value	Explanation
G_n	1 - 15	Density of ECM
G_x	**1**	Pak's effect on Phophorylated paxillin vs. NA turnover
E_n	**10**	Protrusion response to Rac
E_s	**0.1**	Myosin mediated adhesion maturation
P_o	**0.01**	Pak activity in absence of adhesion
K_p	**0.1**	Saturation of Rac-mediated Pak activation
C_n	**0.1**	Turnover of adhesions in absence of ECM
C_r	**0** - 0.02	Inhibition of Rac due to GAP activity
I_n	**0** - 0.02	Inhibition of protrusion by stable adhesions
L_m	0.1 - **1**	Diffusion rate of Myosin
L_r	**0.1** - 1	Diffusion rate of Rac
L_g	**0.1** - 1	Diffusion rate of GAP

3.2.4 Derivation of parameters for stochastic model

To the extent possible, we expressed the parameters in equations 3.1 – 3.8 in terms of the dimensionless parameters, so direct comparison between the stochastic model and the bifurcation analysis could be made.

$$k_{a,NA}^{ECM} = \frac{G_n^{ECM} k_{d,NA} NA^{\dagger}}{K_o} \tag{3.36}$$

$$K_{inhibit} = \frac{I_n k_{d,SA}}{C_n k_{d,NA} NA^{\dagger}} \tag{3.37}$$

$$k_{mature} = C_n k_{d,NA} \tag{3.38}$$

$$k_{a,Myo} = \frac{E_s k_{d,Myo}}{K_{contract} NA^{\dagger}} \tag{3.39}$$

$$k_{a,Pax} = G_x k_{d,Pax} K_{turnover} \tag{3.40}$$

$$Pak_o = \frac{P_o}{K_{turnover}} \tag{3.41}$$

$$k_{a,Rac} = \frac{E_n K_o G_x K_{turnover} K_p k_{d,rac}}{K_{PA}} \tag{3.42}$$

$$k_{a,Pak} = \frac{K_p K_{PA} k_{d,Pak}}{E_n K_o} \tag{3.43}$$

$$k_{a,GAP} = \frac{C_r k_{d,GAP} k_{d,SA}}{K_{GAP} C_n k_{d,NA} NA^{\dagger}} \tag{3.44}$$

$$D_{Myo} = L_m^2 k_{d,Myo} \tag{3.45}$$

$$D_{Rac} = L_r^2 k_{d,Rac} \tag{3.46}$$

$$D_{GAP} = L_g^2 k_{d,GAP} \tag{3.47}$$

3.2.5 Estimation of non-dimensionless variables

The half life of nascent adhesions in Chinese hamster ovary (CHO) cells is ~30 seconds, while the half life of stable adhesions is on the order of 10 minutes (Nayal et al., 2006). Accordingly, we set $k_{d,NA} = 0.03\ s^{-1}$ and $k_{d,SA} = 0.001\ s^{-1}$. The dissociation constant of Rac has been measured to be $0.067\ s^{-1}$ (Moissoglu et al., 2006). The life times of the other complexes (myosin, phosphorylated-paxillin, GAP and Pak) are assumed to be much shorter, and so we set their dissociation constants to an arbitrary value of $0.3\ s^{-1}$ (Table 3.2). Concentration refers to number of molecules per spatial interval (subvolume).

Table 3.2 Table of parameters in the stochastic model.

Parameter	Value	Units
$k_{d,NA}$	0.03	1/second
$k_{d,SA}$	0.001	1/second
$k_{d,Myo}$	0.3	1/second
$k_{d,Pax}$	0.3	1/second
$k_{d,Rac}$	0.067	1/second
$k_{d,Pak}$	0.3	1/second
$k_{d,GAP}$	0.3	1/second
K_o	3	1/concentration
K_{PA}	3	dimensionless
$K_{turnover}$	10	1/concentration
$K_{contract}$	0.5	1/concentration
K_{GAP}	0.1	1/concentration

3.3 MATERIALS AND METHODS

3.3.1 XPPAUT

XPP is a simple software for solving ordinary differential equations. It also includes a bifurcation analysis program, AUTO, so the package is commonly referred to as XPPAUT. We used this software for bifurcation analysis of our dimensionless, single compartment model. The integrated stiff differential equation solver was used. The code and all pertinent parameters are shown in Appendix A. In the bifurcation analysis we varied parameter Gn (i.e. strength of ECM) and calculated steady state values of all the species in the system. The analysis was performed numerous times with different settings of the negative feedback loops.

3.3.2 Gillespie Algorithm

Gillespie algorithm is a method for numerically simulating the stochastic time evolution of coupled chemical reactions. It was developed by Daniel Gillepsie in 1976 to simulate stochastic chemical and biochemical systems (Gillespie, 1976). The algorithm is particularly useful for simulating systems where the numbers of molecules are low. Mathematically, it is a variation of the dynamic Monte Carlo method. In the

algorithm, all reactions are expressed as system of simple first order chemical reactions. The algorithm consists of the following steps (Gillespie, 1977):

1. Initialization: Initialize the number of molecules in the system and reaction constants.
2. Propensity rate calculation: Calculate the sum of propensities (a) for all reactions based on the current state of the system.

   $$a = \sum_{j=1}^{M} \alpha_j \qquad (3.48)$$

   where α_j is the propensity for reaction j and M is the number of reactions in the system. The propensity for each reaction depends on the stochiometry. For example, the propensity for reaction $S_1 \rightarrow S_2$ with rate constant k_1 would be calculated:

   $$\alpha_i(X(t)) = k_1 X_1(t) \qquad (3.49)$$

   where $X_1(t)$ is the number of molecules of species S_1 at time t.
3. Reaction time step (τ) calculation: Generate random number (*rand*1) and calculate next reaction time.

   $$\tau = \frac{-\ln(rand1)}{a} \qquad (3.50)$$

4. Reaction selection: Generate another random number (*rand*2) and select which reaction will occur next according to:

   $$\sum_{i=1}^{selected} \alpha_i(X(t)) \le (rand2) \sum_{i=1}^{N} \alpha_i(X(t)) \le \sum_{i=1}^{selected+1} \alpha_i(X(t)) \qquad (3.51)$$

5. System update: Update the number of molecules in the system based on the reaction that occurred.
6. Iterate: Go to step 2, unless the total time limit has been reached.

The above described variation of the Gillespie algorithm is also known as the direct method. Since the direct method is computationally demanding, multiple modifications have been made to increase its performance (Bernstein, 2005; Gibson and Bruck, 2000; McCollum et al., 2006).

3.3.3 Next subvolume method

The direct method is not suitable for simulating reaction-diffusion systems; in contrast, the next subvolume method is efficient for systems with a large number of spatial compartments (Elf and Ehrenberg, 2004; Hattne et al., 2005). A schematic of this method is shown in Figure 3.2. The major steps in the next subvolume method are:

Initialization

1. Generate a connectivity matrix that describes the geometry of the system.
2. Distribute initial numbers of molecules in the system and store them in the configuration matrix.
3. Calculate the sum of reaction rates (r_i) and diffusion rates (s_i) for each subvolume and store it in the rate matrix.

$$r_i = \sum_{j=1}^{M} k_j X_i^j \tag{3.52}$$

$$s_i = n_i \sum_{j=1}^{M} d_j X_i^j \tag{3.53}$$

where k_j is the rate constant and d_j is the diffusion rate constant for species j. X_i^j is the number of molecules of species j in subvolume i. M is the number of species, and n_i is the number of directions in which the molecules can diffuse.

4. For each subvolume sum the reaction and diffusion rates, generate a random number (*rand*) uniformly distributed between 0 and 1, and calculate the first event time (τ_i).

$$\tau_i = \frac{-\ln(rand)}{r_i + s_i} \tag{3.54}$$

5. Order the subvolumes according to their next event times. The subvolumes are kept in a sorted array (an event queue) so that the subvolume for which the event occurs first is on top.

Iterations

6. For the subvolume with smallest next event time (subvolume λ, first in event queue) a random number is generated to determine whether reaction or diffusion step will occur.

If, $rand < \frac{r_\lambda}{r_\lambda + s_\lambda}$ (3.55)

a reaction event will occur. Otherwise, a diffusion event will occur.

7. Reaction event:
   a) Generate a random number to determine which reaction will occur (as in the direct method).
   b) Update the number of molecules in the subvolume.
   c) Recalculate reaction (r_λ) and diffusion rates (s_λ) for subvolume λ, generate random number, and calculate the time of the next event.

$$\tau_\lambda = \frac{-\ln(rand)}{r_\lambda + s_\lambda} + t \quad (3.56)$$

   d) Insert the new event time of subvolume λ into the event queue and order the queue.
8. Diffusion event:
   a) Generate a random number to determine which type of molecule diffused away.
   b) Direction of diffusion is chosen by randomly selecting a column in the connectivity matrix.
   c) Update the states in subvolume λ and in the subvolume where the molecule diffused (subvolume γ).
   d) Recalculate reaction and diffusion rates for subvolumes λ and γ.
   e) Generate next event times for subvolumes λ and γ.
   f) Insert new event times of subvolumes λ and γ into the event queue and order the queue.
9. Return to step 6, for the next iteration until the specified time limit is reached.

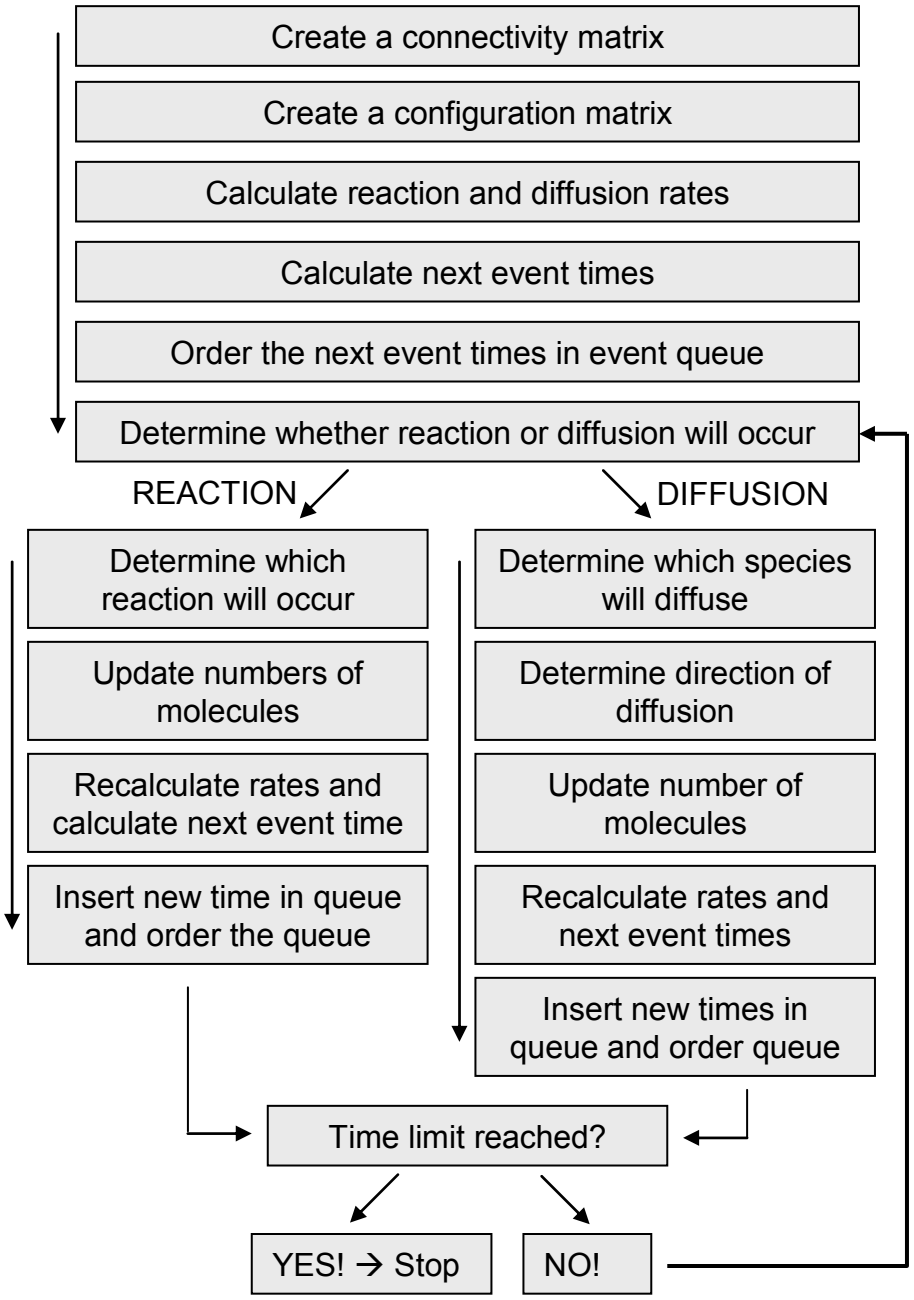

Figure 3.2 Schematic of the next subvolume method. The steps are executed from top to bottom according to the arrows.

3.4 RESULTS

3.4.1 Bifurcation analysis

We performed a bifurcation analysis in XPPAUT software to explore possible steady states depending on the density of ECM. Two direct negative feedback loops can be adjusted in the model: inhibition of Rac activity by GAP and inhibition of protrusion as a result of stable adhesions (see Fig. 3.1). We varied the strength of these negative feedback loops to determine their effect on the steady states. It should be noted that a third, indirect mode of regulation is present in all cases: positive feedback that enhances the rate of maturation from nascent to stable adhesions (Fig. 3.1).

The analysis revealed multiple steady states at intermediate ECM concentrations in the absence of either negative feedback loop (Fig. 3.3). At low ECM density, few nascent adhesions are formed, resulting in lack of Rac/Pak signaling. At intermediate ECM density, nascent adhesions are formed readily, increasing Rac/Pak signaling and membrane protrusion.

In the presence of the GAP negative feedback loop, multiple steady states are present at two intervals of ECM density (Fig. 3.4). These intervals are highly dependent on the parameter C_r (strength of GAP feedback), and the multiple steady states are not present when the GAP feedback loop is too strong (data not shown).

When inhibition of protrusion by stable adhesion is included, multiple steady states are still present at intermediate density of ECM (Fig. 3.5). The multiple steady state window is similar to the case without inhibition (shown in Fig. 3.3).

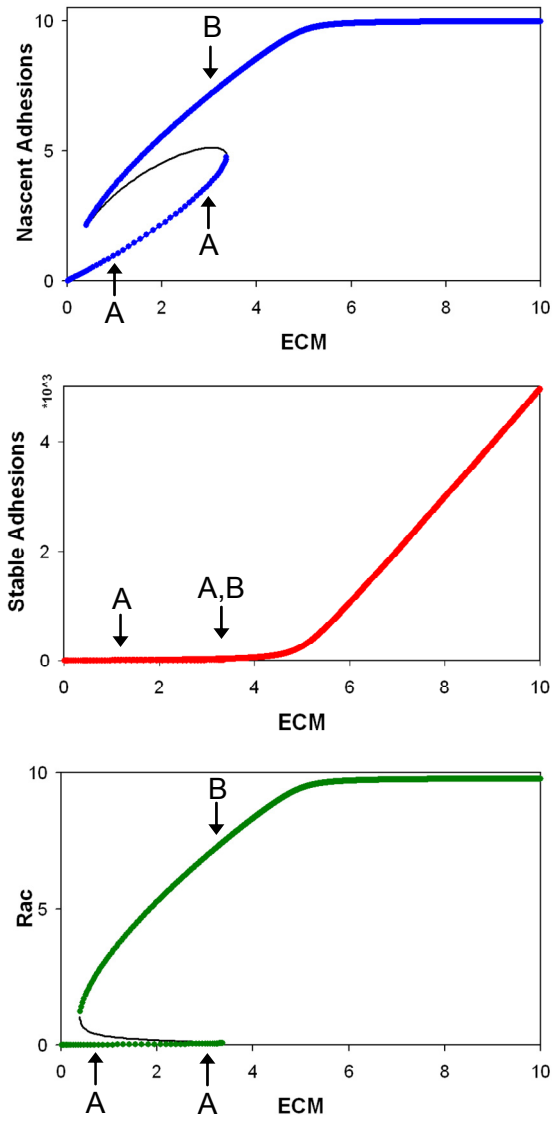

Figure 3.3 Bifurcation diagrams with negative feedbacks turned off. Thick colored lines represent stable steady states. Thin black lines represent unstable steady states. A – state of low adhesion and low signaling. B – State of high adhesion and high signaling with the absence of many stable adhesions. Parameter Settings: I_n=0 C_r=0

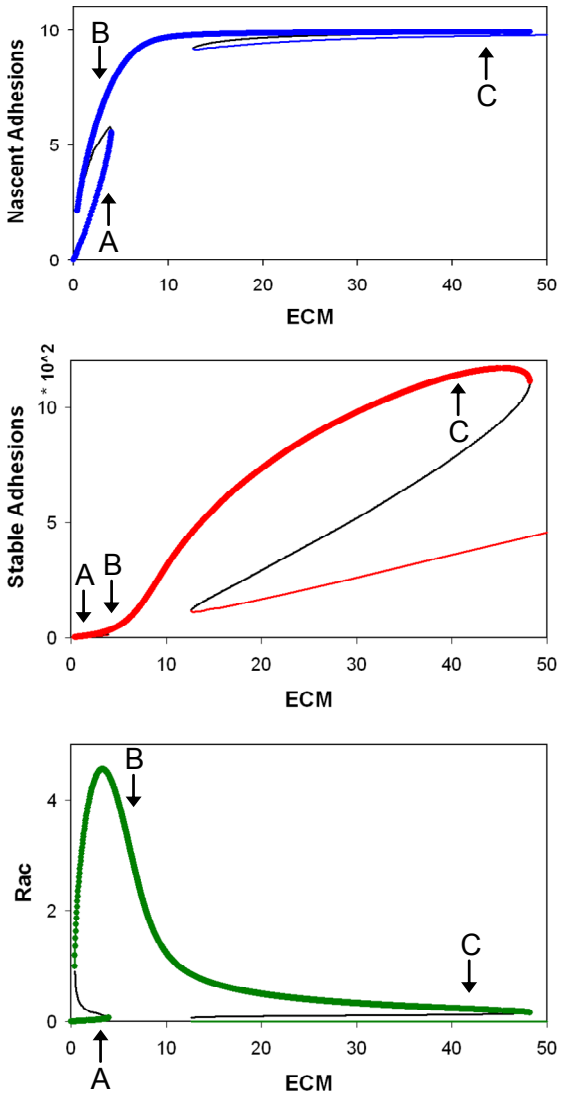

Figure 3.4 Bifurcation diagrams with GAP negative feedback loop. Thick colored lines represent stable steady states. Thin black lines represent unstable steady states. A – state of low adhesion and low signaling. B – State of high adhesion and high signaling with the absence of many stable adhesions. C – State of high adhesion, low signaling and high adhesion maturation. Parameter Settings: I_n=0 C_r=0.02

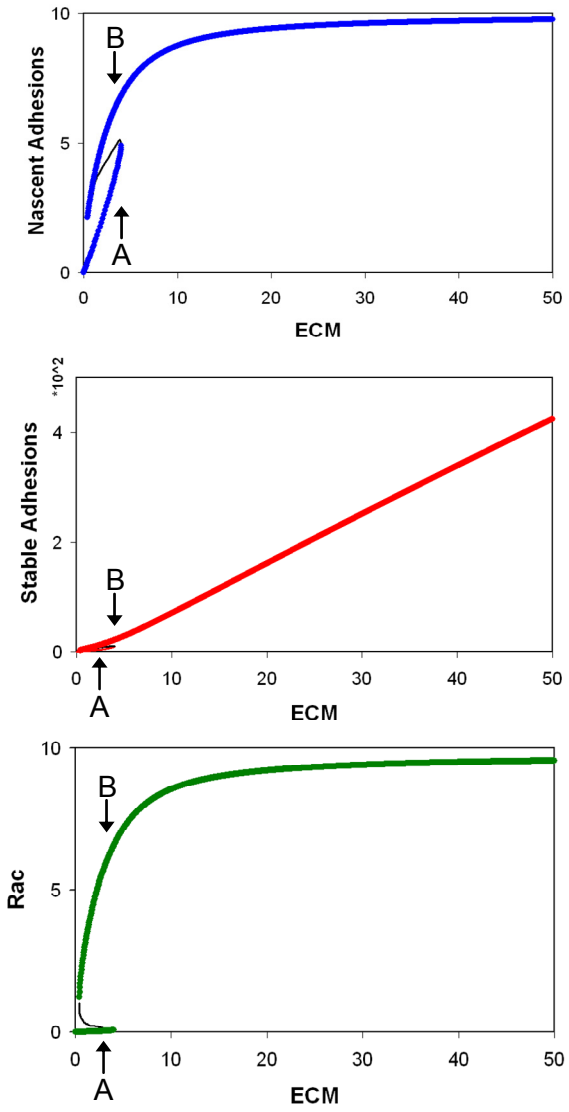

Figure 3.5 Bifurcation diagrams with protrusion inhibition induced by stable adhesions. Thick colored lines represent stable steady states. Thin black lines represent unstable steady states. A – state of low adhesion and low signaling. B – State of high adhesion and high signaling with the absence of many stable adhesions. Parameter Settings: I_n=0.02 C_r=0

In Figures 3.3 – 3.5 we point to three common states of the leading edge. State A is characterized by low adhesion and low Rac/Pak signaling. In state B, many nascent adhesions are present, resulting in high Rac/Pak signaling, while maturation of adhesions is low. In state C, nascent adhesions mature at a higher rate, which can result

in low levels of Rac/Pak signaling if the GAP feedback is sufficiently strong. These states are graphically represented in Figure 3.6.

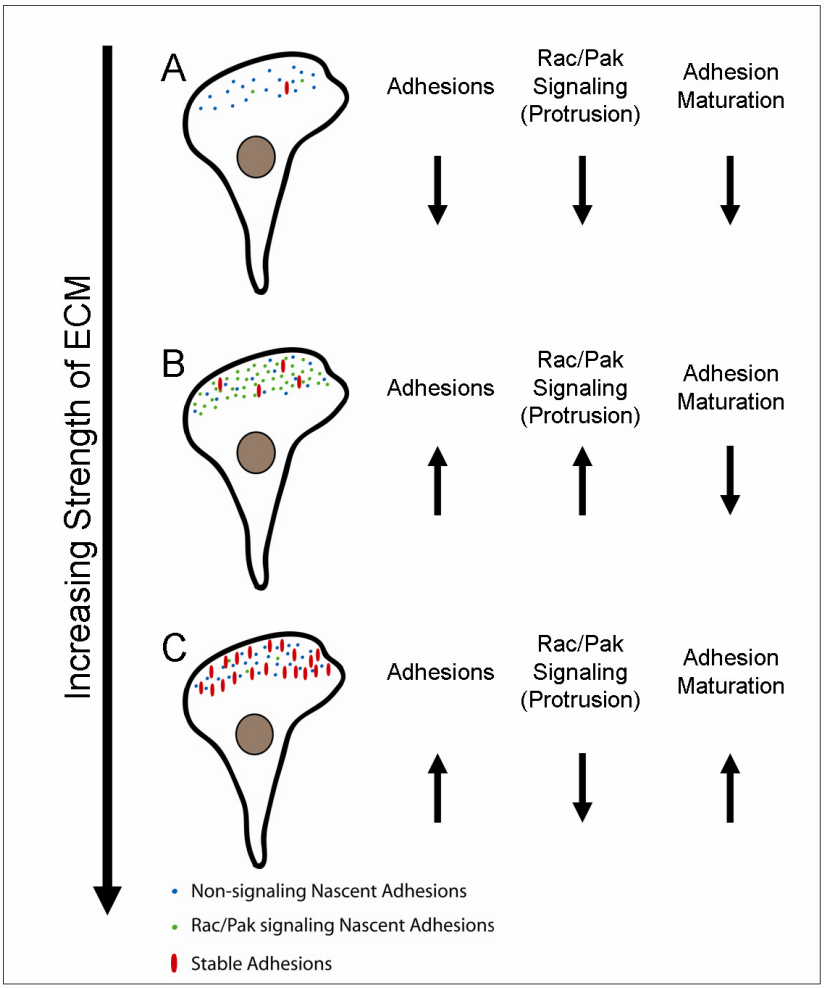

Figure 3.6 Different states of signaling molecules at the leading edge. A – state of low adhesion and low signaling. B – State of high adhesion and high signaling with the absence of many stable adhesions. . C – State of high adhesion, low signaling and high adhesion maturation.

3.4.2 Dependence of leading edge dynamics on ECM density

In the bifurcation analysis, we assess the effect of ECM density on steady-state levels of signaling molecules, where the leading edge is modeled as one, well-mixed compartment. In the stochastic model, the leading edge is treated as a one-dimensional arc divided into 30 subvolumes and molecules, can diffuse between them. The system is

constantly changes, so a true steady state can not be achieved. However, when the simulation is carried out for a long period of time, the system changes slowly. We call this a "quasi-steady" state. System in the quasi-steady state is still dynamic but the magnitude of fluctuations is small in time.

The parameter G_n reflects the density of ECM in the model. Quasi-steady states for four different values of G_n are shown in Figure 3.7. At low ECM densities (G_n = 1 and 3.3) adhesion is low, resulting in a lack of signaling and maturation. Adhesion increases at certain parts of the leading edge for higher ECM density (G_n = 8 and 15). Different states of activation (shown in Fig. 3.6) coexist at the same time in the leading edge (states are marked A, B, and C).

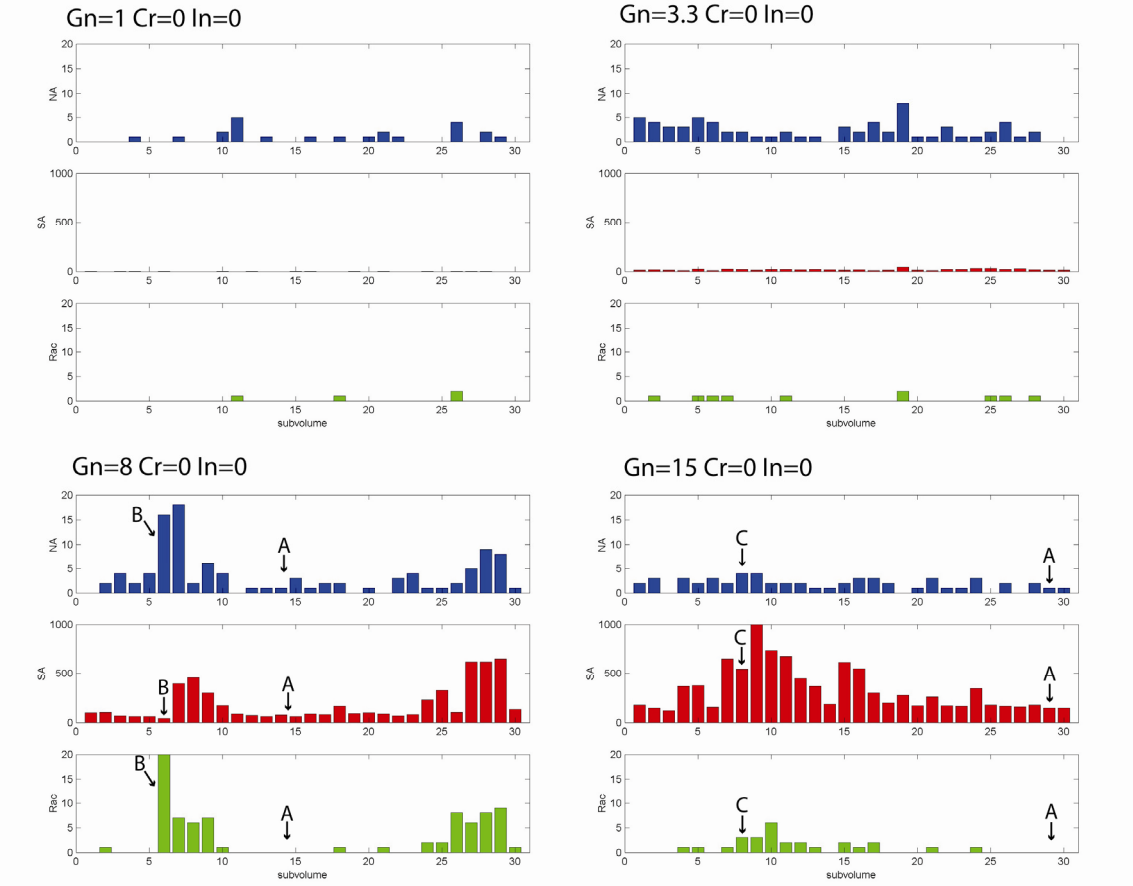

Figure 3.7 Effect of ECM density on leading edge dynamics. Quasi-steady states for different densities of ECM are shown. Both negative feedback loops are turned off (C_r=0 I_n=0). ECM density has a major effect on leading edge dynamics. The y-axis shows number of molecules per subvolume. Different states are marked A, B and C.

3.4.3 Effect of negative feedback loops on leading edge dynamics

In our model, we have the capability to adjust the strength of negative feedback loops. The bifurcation analysis revealed the importance of inhibition on steady states of the system. The effects of inhibitory pathways on the stochastic model are shown in Figure 3.8. Either negative feedback loop essentially shuts down the signaling at the leading edge, resulting in more uniform levels of stable adhesions.

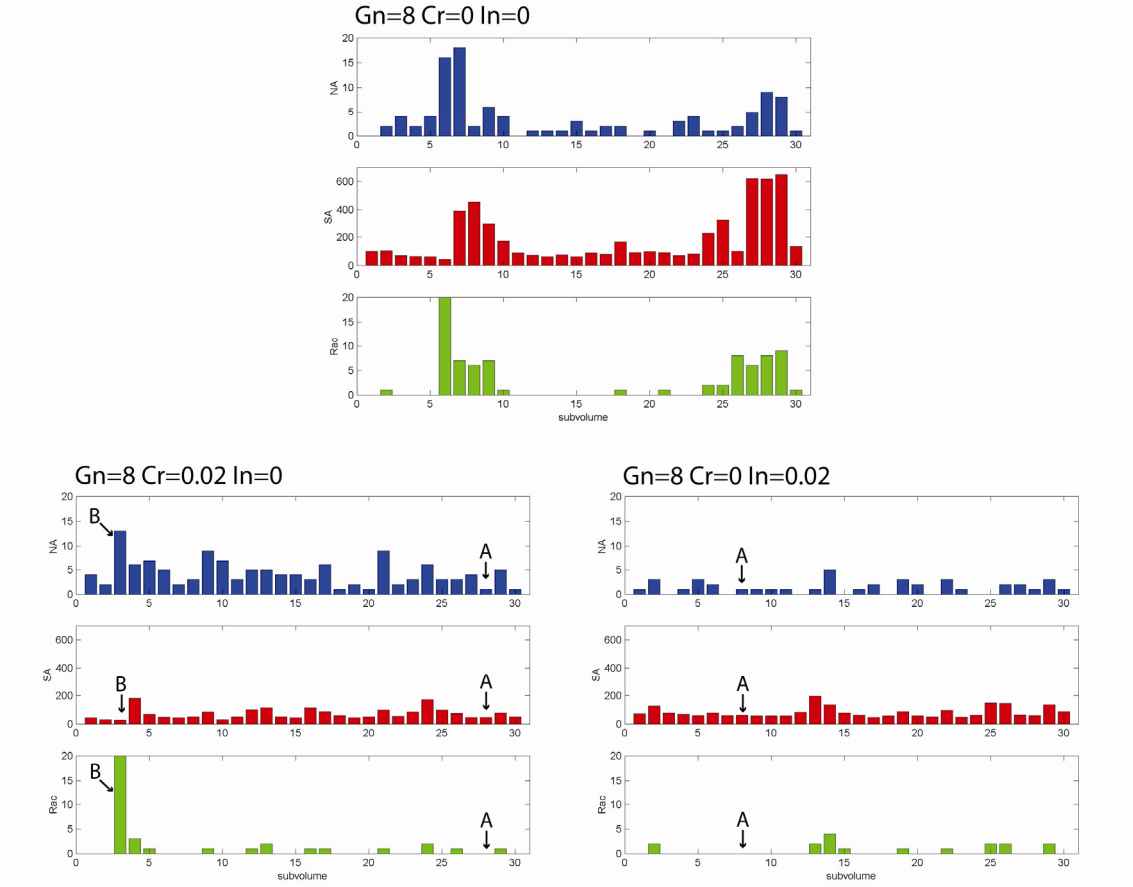

Figure 3.8 Effect of inhibition on leading edge dynamics. Quasi-steady states are shown when GAP inhibition is present (C_r=0.02) or when protrusion inhibition is turned on (I_n=0.02). Either type of inhibition results in less heterogeneity at the leading edge when quasi-steady state is reached. The y-axis shows number of molecules per subvolume. Different states are marked A, B and C.

3.4.4 Effect of Rac diffusion on leading edge dynamics

As mentioned in the Introduction, myosin acts at a distance by pulling on actin fibers that are connected to focal adhesion. To model this global effect, we set the diffusion rate of myosin to be ten times higher than for Rac and GAP. However, Rac can also diffuse at the leading edge. We increased the diffusion rate of Rac ten fold in the stochastic model to explore its effect. Quasi-steady states for low and high Rac diffusion are shown in Figure 3.9. Increasing the Rac diffusion rate decreases the heterogeneity in signaling between the subvolumes.

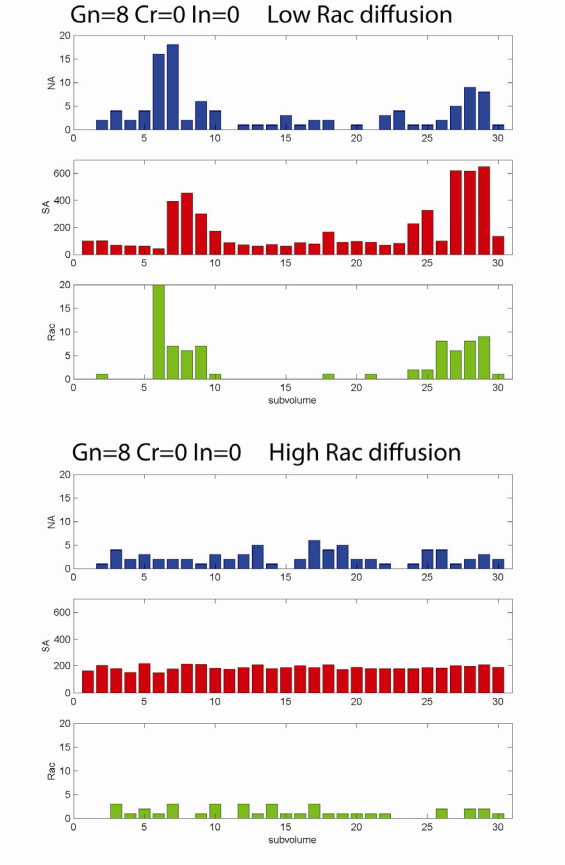

Figure 3.9 Effect of Rac diffusion rate on leading edge dynamics. Quasi-steady states for low (top) and high (bottom) Rac diffusion are shown. Increase in Rac diffusion decreases the differences between the subvolumes, making the leading edge signaling more homogeneous. Both negative feedback loops are turned off (C_r=0 I_n=0). The y-axis shows number of molecules per subvolume.

3.4.5 Evolution of leading edge dynamics in time

All of the previous figures show the system at steady or quasi-steady state. The biggest advantage of the stochastic model is that we can examine the leading edge dynamics at different time points. In Fig. 3.10 we show the levels of molecules at four different time points, with Rac inhibition by GAP (C_r = 0.02). At the beginning (time = 50) many nascent adhesions are formed as a response to ECM but Rac/Pak signaling is at low levels. When more nascent adhesions are formed (time = 125) the positive Rac/Pak signaling is activated, resulting in more nascent adhesions. Great number of adhesions results in formation of stable adhesion, which triggers the GAP negative feedback loop (time = 215). Once sufficient number of stable adhesions is formed the

maturation process is further enhanced, resulting in decrease of protrusion ad nascent adhesions (time = 500). Lack of protrusion converts the 'leading' edge into a stable edge. A new leading edge will be formed somewhere else in the cell.

Similar behavior is observed for inhibition of protrusion by stable adhesions instead of the Rac inhibition by GAP (Fig. 3.11). However, formation of many stable adhesions eliminates protrusion but does not abolish Rac signaling.

Figure 3.10 Leading edge dynamics with GAP negative feedback loop. Molecule levels in the leading edge are shown at four different time points (time has arbitrary units). Inhibition of Rac by GAP is present (C_r=0.02). The y-axis shows number of molecules per subvolume. Different states are marked A, B and C.

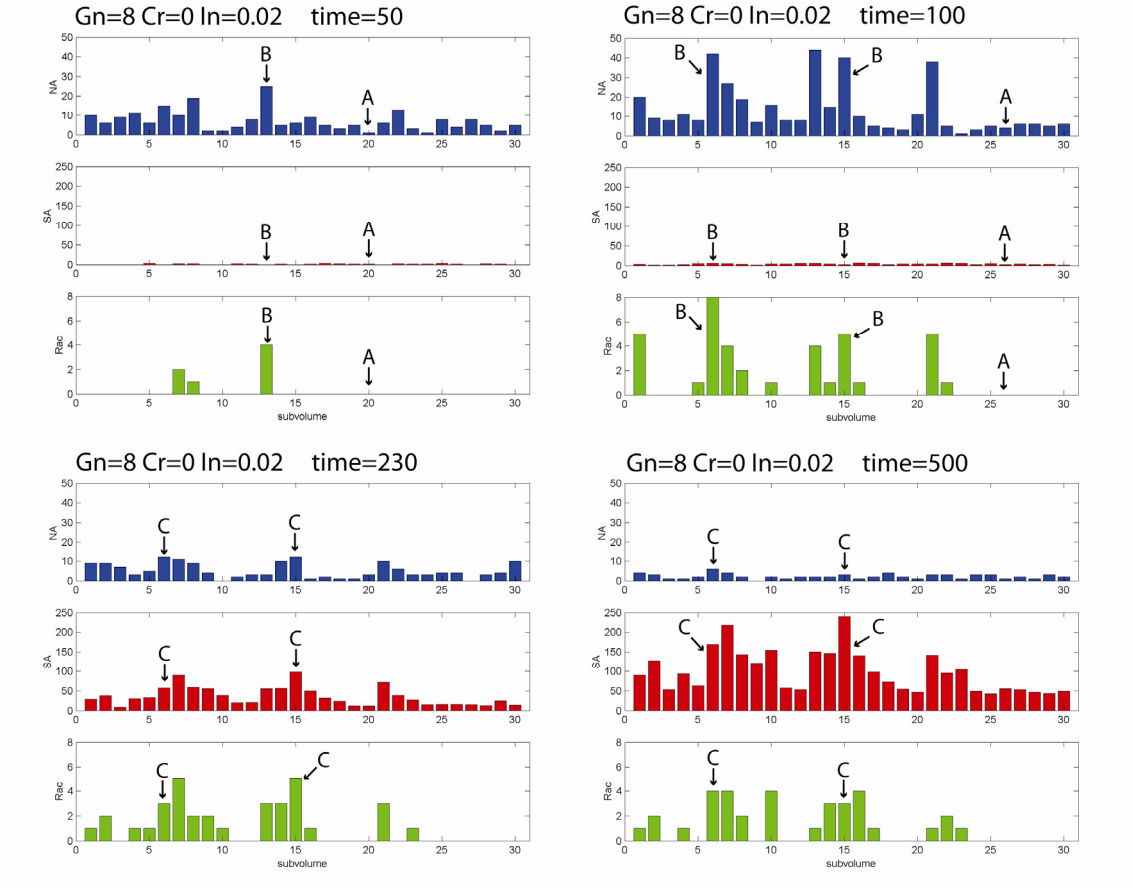

Figure 3.11 Leading edge dynamics with inhibition of protrusion by stable adhesion. Molecule levels in the leading edge are shown at four different time points (time has arbitrary units). Inhibition of protrusion by stable adhesions is present (I_n=0.02). The y-axis shows number of molecules per subvolume. Different states are marked A, B and C.

3.5 DISCUSSION

We have developed a model for signaling at the leading edge of migrating cells. We expressed the model as a series of differential equations and performed a bifurcation analysis to examine steady states at different densities of ECM. Multiple steady states are present at intermediate ECM densities. In the bifurcation analysis, leading edge was modeled as one compartment, eliminating the effects of diffusion. We predicted that if the leading edge would be divided into multiple compartments, different steady states could be present at neighboring compartments.

To explore this possibility, we developed a stochastic model with thirty subvolumes, allowing to study the effects of diffusion. We present the quasi-steady states for various parameter settings and show that different states of signaling can be present in the leading edge at the same time. We also show the effects of various inhibitory pathways on the overall response of the system.

The model output can be compared to experimental data. Dynamics of nascent and stable adhesions can be examined in motile cells transfected with EGFP-Paxillin by TIRF microscopy. In our model, the species NA is defined as nascent adhesions bound to paxillin. The nascent adhesions mature into stable adhesions bound to paxillin. Therefore, the signal of EGFP-Paxillin from TIRF images can be compared to the levels of NA and SA. Nascent adhesions are turned over rapidly, so they will look as flicker in the TIRF videos. Large, bright spots that are not moving much in time will represent stable adhesions.

Similar experiments could be done with cells transfected with EGFP-Rac since active GTP-bound Rac is recruited to the membrane. The levels of fluorescence could be compared to the levels of Rac in the model. Ideally, paxillin and Rac could be studied experimentally at the same time if each protein was tagged by different fluorescent protein.

3.6 REFERENCES

Bernstein, D. 2005. Simulating mesoscopic reaction-diffusion systems using the Gillespie algorithm. *PHYSICAL REVIEW E*. 71:-.

DiMilla, P., K. Barbee, and D. Lauffenburger. 1991. Mathematical-model for the effects of adhesion and mechanics on cell-migration speed. *BIOPHYSICAL JOURNAL*. 60:15-37.

Elf, J., and M. Ehrenberg. 2004. Spontaneous separation of bi-stable biochemical systems into spatial domains of opposite phases. *SYSTEMS BIOLOGY*. 1:230-236.

Gibson, M., and J. Bruck. 2000. Efficient exact stochastic simulation of chemical systems with many species and many channels. *JOURNAL OF PHYSICAL CHEMISTRY A*. 104:1876-1889.

Gillespie, D. 1976. General method for numerically simulating stochastic time evolution of coupled chemical-reactions. *JOURNAL OF COMPUTATIONAL PHYSICS*. 22:403-434.

Gillespie, D. 1977. Exact stochastic simulation of coupled chemical-reactions. *JOURNAL OF PHYSICAL CHEMISTRY*. 81:2340-2361.

Gupton, S., and C. Waterman-Storer. 2006. Spatiotemporal feedback between actomyosin and focal-adhesion systems optimizes rapid cell migration. *CELL*. 125:1361-1374.

Hattne, J., D. Fange, and J. Elf. 2005. Stochastic reaction-diffusion simulation with MesoRD. *BIOINFORMATICS*. 21:2923-2924.

McCollum, J., G. Peterson, C. Cox, M. Simpson, and N. Samatova. 2006. The sorting direct method for stochastic simulation of biochemical systems with varying reaction execution behavior. *COMPUTATIONAL BIOLOGY AND CHEMISTRY*. 30:39-49.

Moissoglu, K., B. Slepchenko, N. Meller, A. Horwitz, and M. Schwartz. 2006. In vivo dynamics of Rac-membrane interactions. *MOLECULAR BIOLOGY OF THE CELL*. 17:2770-2779.

Nayal, A., D. Webb, C. Brown, E. Schaefer, M. Vicente-Manzanares, and A. Horwitz. 2006. Paxillin phosphorylation at ser273 localizes a GIT1-PIX-PAK complex and regulates adhesion and protrusion dynamics. *JOURNAL OF CELL BIOLOGY*. 173:587-599.

Palecek, S., J. Loftus, M. Ginsberg, D. Lauffenburger, and A. Horwitz. 1997. Integrin-ligand binding properties govern cell migration speed through cell-substratum adhesiveness. *NATURE*. 385:537-540.

Pestonjamasp, K., C. Forster, C. Sun, E. Gardiner, B. Bohl, O. Weiner, G. Bokoch, and M. Glogauer. 2006. Rac1 links leading edge and uropod events through Rho and myosin activation during chemotaxis. *BLOOD*. 108:2814-2820.

Vicente-Manzanares, M., J. Zareno, L. Whitmore, C. Choi, and A. Horwitz. 2007. Regulation of protrusion, adhesion dynamics, and polarity by myosins IIA and IIB in migrating cells. *JOURNAL OF CELL BIOLOGY*. 176:573-580.

Appendices

APPENDIX A: XPPAUT CODE

```
# We have 7 different chemical species that need to be solved for:
# n = Nascent Adhesions
# s = Stable Adhesions
# m = Myosin
# x  = Paxillin
# r  = Rac
# g = GAP
# p = PAK

# ..... ODEs START .....
n'=k_d_NA*((G_n*((1+(E_n*r))/(1+(I_n*s))))-((1+p+(C_n*(1+(E_s*m))))*n))
s'=k_d_SA*(((1+(E_s*m))*n)-s)
m'=k_d_Myo*(s-m)
x'=k_d_Pax*((G_x*(P_o+p)*(n-x))-x)
r'=k_d_Rac*(x-(r*(1+(C_r*g))))
g'=k_d_GAP*(s-g)
p'=k_d_PAK*((r*(x-(K_p*p)))-p)

# ..... ODEs END .....


# ---------- START OF PARAMETERS ----------

# Dimensionless Parameters are denoted by capital letters with subscripts

# "G_n" is the bifurcation parameter that depends on ECM
# "P_o" is PAK activity in the absence of adhesions (low)
# "K_p" saturation of Rac-mediated PAK activation
par G_n=0.01,P_o=0.01,K_p=0.1,G_x=1

# "C" stands for "consumption"
# C_n When adhesion strength is low, most NAs turn over rather than mature
# C_p Parameter that compares PAK's influence on NA turnover relative to its influence
on paxillin phosphorylation
par C_n=0.1,C_r=0

# "E" stands for "enhancement"
# "E_n" Protrusion responds robustly to Rac signaling
# "E_s" Effect of stable adhesions on actomyosin-mediated adhesion maturation
par E_n=10,E_s=0.1

# "I" stands for "inhibition"
```

```
# "I_n" Effect of stable adhesion on inhibition of protrusion
par I_n=0

% Dissociation constants:
par
k_d_NA=1,k_d_SA=1,k_d_Myo=1,k_d_Pax=1,k_d_Rac=1,k_d_GAP=1,k_d_PAK=1

# ---------------------- END OF PARAMETERS -----------------------------

# Defines Initial Conditions
init n=0,s=0,m=0,x=0,r=0,g=0,p=0

# total means the range of t for integration (tspan)
@ total=100

# METH indicates the method of integration
@ METH=stiff

# dt indicates the integration step
@ dt=0.05

# bound indicates the maximum value that a parameter can reach during integration
@ bound=1.e100

# xp indicates variable on x axis; yp indicates variable on y axis; the rest defines the
plotting window
@ xp=t,yp=x,xlo=0,xhi=100,ylo=0,yhi=10
done
```

APPENDIX B: MATLAB CODE

```
function intergrin_next_subvolume_v17

% This is a stochastic version of the integrin model that uses the next subvolume
method
% There are 14 reactions:
% Reaction  1: Formation of nascent adhesions as a response to protrusion
%           Result: N-->N+1
% Reaction  2: Turnover of Nascent Adhesions
%           Result: N-->N-1
% Reaction  3: Maturation of Nascent Adhesions
%           Result: N-->S (N-->N-1 & S-->S+1)
% Reaction  4: Dissociation of Stable Adhesions
%           Result: S-->S-1
% Reaction  5: Activation of Myosin due to Stable Adhesions
%           Result: M-->M+1
% Reaction  6: Deactivation of Myosin
%           Result: M-->M-1
% Reaction  7: Activation of Paxillin
%           Result: X-->X+1
% Reaction  8: Deactivation of Paxillin
%           Result: X-->X-1
% Reaction  9: Activation of Rac due to paxillin
%           Result: R-->R+1
% Reaction 10: Deactivation of Rac
%           Result: R-->R-1
% Reaction 11: Activation of GAP due to Stable Adhesions
%           Result: G-->G+1
% Reaction 12: Deactivation of GAP
%           Result: G-->G-1
% Reaction 13: Activation of PAK due to Rac
%           Result: P-->P+1
% Reaction 14: Deactivation of PAK
%           Result: P-->P-1

% ------------------------------------------------------------------------------
timelimit=200;                % Length of running time
data_write_frequency_tau=(timelimit/1000); % Determines how frequently data are
stored (e.g. frequency_tau=0.01, writes point every 0.01 in time)
loop_limit=100000;   % Length of running time (in number of loops)
```

```
data_write_frequency=100;   % Determines how frequently data are stored (e.g. if it is
100, very 100th point is stored)

% PARAMETERS - Dimensionless Variables (same as in the bifurcation analysis)
Gn = 8;
En = 10;
In = 0.02;
Cn = 0.1;
Es = 0.1;
Gx = 1;
Po = 0.01;
Cr = 0;
Kp = 0.1;
Lm = 1;         % DIFFUSION Parameter - MYOSIN
Lr = 0.1;       % DIFFUSION Parameter - Rac
Lg = 0.1;       % DIFFUSION Parameter - GAP

% PARAMETERS - Dissociation Constants
kd_NA = 0.03;
kd_SA = 0.001;
kd_myo = 0.3;
kd_pax = 0.3;
kd_GAP = 0.3;
kd_PAK = 0.3;
kd_Rac = 0.067;

% PARAMETERS - OTHER 5 CONSTANTS THAT NEED TO BE SPECIFIED
(these were not in the bifurcation model)
K_o = 3;
K_PA = 3;
K_turnover = 10;
K_contract = 0.5;
K_GAP = 0.1;

% CALCULATED PARAMETERS
D_myo = (Lm^2)*kd_myo;
D_Rac = (Lr^2)*kd_Rac;
D_GAP = (Lg^2)*kd_GAP;

k_mature = Cn*kd_NA;
PAKo = (Po/K_turnover);

ka_pax = Gx*kd_pax*K_turnover;
ka_Rac = (En*K_o*kd_Rac*ka_pax*Kp)/(kd_pax*K_PA);
```

```
ka_PAK = (Kp*kd_PAK*K_PA)/(En*K_o);

NA_cross = ((kd_pax*kd_Rac*kd_PAK)/(ka_pax*ka_Rac*ka_PAK))^(1/2);

ka_myo = (Es*kd_myo)/(K_contract*NA_cross);
ka_GAP = (Cr*kd_GAP*kd_SA)/(K_GAP*Cn*kd_NA*NA_cross);
K_inhibit = (In*kd_SA)/(Cn*kd_NA*NA_cross);

ka_NA_ECM = (Gn*kd_NA*NA_cross)/K_o;

%-----CONNECTIVITY MATRIX----------------------------------------------------------------
% This file defines the connectivity matrix used in the next subvolume algorithm.
% Each row in the matrix corresponds to one subvolume.
% There are 6 columns in each row that specify the neighbor subvolume:
%     1 - Left
%     2 - Right
%     3 - Up
%     4 - Down
%     5 - Into the screen
%     6 - Away from the screen

% There are 30 subvolumes in one dimension
%  | 1 | 2 | 3 | 4 | 5 | 6 | 7 | 8 | 9 | 10 |.....|29|30|

conn_matrix = xlsread('conn_matrix_1D_30row_openbound.xls');  % The connectivity
matrix is loaded from the specified Excel file

conn_matrix_size = size(conn_matrix);
dimension = conn_matrix_size(1,2);     % This determines the dimension of the system
(i.e. in how many directions can a molecule diffuse)
                                % 1D geometry: Dimension = 2
                                % 2D geometry: Dimension = 4
                                % 3D geometry: Dimension = 6

%-----------------------------------------------------------------------------------------
--


%-----CONFIGURATION MATRIX----------------------------------------------------------------
----------

% This file defines the configuration matrix used in the next subvolume algorithm.
% Each row in the matrix corresponds to one subvolume.
```

```
% The columns within each row represent the current population of the particular
species.

c_m = xlsread('config_matrix_30row.xls');  % The initial configuration matrix is loaded
from a Excel file

size_c_m=size(c_m);
subvolumes=size_c_m(1,1);  % This specifies now many subvolumes are in the system

%-----------------------------------------------------------------------------------------------
--


%-----RATE MATRIX-------------------------------------------------------------------------------
-----------
% The propensities (reaction rates) for each reaction are calculated below

%                                'Rac'                        'SA'
a1_matrix = ka_NA_ECM*((K_o+(K_PA * c_m(:,5) )) ./ (1+(K_inhibit * c_m(:,2)  )));
%                               'Pak'       'NA'
a2_matrix=kd_NA*(1+(K_turnover* c_m(:,7) )) .*  c_m(:,1);
%                                'Myo'        'NA'
a3_matrix=k_mature*(1+(K_contract* c_m(:,3) )) .* c_m(:,1);
%               'SA'
a4_matrix=kd_SA* c_m(:,2);
%               'SA'
a5_matrix=ka_myo* c_m(:,2);
%               'Myo'
a6_matrix=kd_myo* c_m(:,3);
%                     'PAK'         'NA'      'Pax'
a7_matrix=ka_pax*(PAKo + c_m(:,7) ).*( c_m(:,1) - c_m(:,4) );
%               'Pax'
a8_matrix=kd_pax* c_m(:,4);
%               'Pax'
a9_matrix=ka_Rac* c_m(:,4);
%                           'GAP'        'Rac'
a10_matrix=kd_Rac*(1+(K_GAP * c_m(:,6) )).* c_m(:,5);
%                'SA'
a11_matrix=ka_GAP* c_m(:,2);
%                'GAP'
a12_matrix=kd_GAP* c_m(:,6);
%                'Pax'       'PAK'      'Rac'
a13_matrix=ka_PAK*( c_m(:,4) - c_m(:,7 )).* c_m(:,5);
%                'PAK'
```

```
a14_matrix=kd_PAK* c_m(:,7);

a_matrix_SUM =
a1_matrix+a2_matrix+a3_matrix+a4_matrix+a5_matrix+a6_matrix+a7_matrix+a8_mat
rix+a9_matrix+a10_matrix+a11_matrix+a12_matrix+a13_matrix+a14_matrix;

myo_diff_matrix = dimension * D_myo * c_m(:,3);   % This calculates the diffusion
rate for each subvolume
Rac_diff_matrix = dimension * D_Rac * c_m(:,5);
GAP_diff_matrix = dimension * D_GAP * c_m(:,6);

diff_matrix_SUM = myo_diff_matrix + Rac_diff_matrix + GAP_diff_matrix;  % Sum
of all diffusion rates

% r_m == "RATE MATRIX"
r_m = [a_matrix_SUM   diff_matrix_SUM   (a_matrix_SUM+diff_matrix_SUM)];


%-----REACTION TIMES MATRIX-----------------------------------------------------
-----------------
%                  event time                        subV #
tau_matrix = [((-log(rand(subvolumes,1)))./r_m(:,3))    c_m(:,8)];  % The subvolume
number is there just as an ID for the event time

tau_matrix_ordered = sortrows(tau_matrix); % The RATE MATRIX is now sorted
according to the event times


%  initialization

  time_start=clock;   % This is the actual time the code started to run
  time=0;           % The time starts at zero
  loop_num=0;        % This is used as a counter for how many iterations were
performed
  reaction_count=0;   % This is used as a counter for how many reactions were
performed
  diffusion_count=0;  % This is used as a counter for how many diffusion events were
performed
  point=0;           % This is used to write specific points into a wk1 file
  row_num_point=0;    % This is used to specify rows when writing specific points into
a wk1 file
  tau_step=0;
  last_tau=0;
```

```
%-----ITERATIONS----------------------------------------------------------------------------------
-------
while tau_matrix_ordered(1,1) < timelimit  % This is the PRIMARY loop, calculations
are performed until a desired time is reached

   random1=rand(1,1);  % Generates one random number
   top_row = tau_matrix_ordered(1,2);  % Determines which subvolume has the
smallest reaction time (based on ordered tau matrix)

   if random1 < ((r_m(top_row,1))/(r_m(top_row,3))) % This is the SECONDARY
loop, it determines whether reation of diffusion will occur
      %------REACTION EVENT OCCURS------
      reaction_count=reaction_count+1;   % Keeps track of the number of reactions that
were performed

      tau=tau_matrix_ordered(1,1) % This is used when storing the model data

     sum(1)=0;
     sum(2)=0;
     sum(3)=0;
     sum(4)=0;
     sum(5)=0;
     sum(6)=0;
     sum(7)=0;
     sum(8)=0;
     sum(9)=0;
     sum(10)=0;
     sum(11)=0;
     sum(12)=0;
     sum(13)=0;
     sum(14)=0;
     sum(15)=0;  % The sum number is one more than the number of reactions

     % Propensities of the particular reactions

     a1=ka_NA_ECM*((K_o+(K_PA * c_m(top_row,5) )) ./ (1+(K_inhibit *
c_m(top_row,2)  )));
     a2=kd_NA*(1+(K_turnover* c_m(top_row,7) )) .*  c_m(top_row,1);
     a3=k_mature*(1+(K_contract* c_m(top_row,3) )) .* c_m(top_row,1);
     a4=kd_SA* c_m(top_row,2);
     a5=ka_myo* c_m(top_row,2);
     a6=kd_myo* c_m(top_row,3);
     a7=ka_pax*(PAKo+ c_m(top_row,7) ).*( c_m(top_row,1) - c_m(top_row,4) );
     a8=kd_pax* c_m(top_row,4);
```

```
    a9=ka_Rac* c_m(top_row,4);
    a10=kd_Rac*(1+(K_GAP* c_m(top_row,6) )).* c_m(top_row,5);
    a11=ka_GAP* c_m(top_row,2);
    a12=kd_GAP* c_m(top_row,6);
    a13=ka_PAK*( c_m(top_row,4) - c_m(top_row,7 )).* c_m(top_row,5);
    a14=kd_PAK* c_m(top_row,7);

    yr2 = random1 * r_m(top_row,1);

    sum(2)=sum(1)+a1;
    sum(3)=sum(2)+a2;
    sum(4)=sum(3)+a3;
    sum(5)=sum(4)+a4;
    sum(6)=sum(5)+a5;
    sum(7)=sum(6)+a6;
    sum(8)=sum(7)+a7;
    sum(9)=sum(8)+a8;
    sum(10)=sum(9)+a9;
    sum(11)=sum(10)+a10;
    sum(12)=sum(11)+a11;
    sum(13)=sum(12)+a12;
    sum(14)=sum(13)+a13;
    sum(15)=sum(14)+a14;


    for k=2:15
    if (sum(k) >= yr2) & (sum(k-1) < yr2) %THIS DETERMINES WHICH
REACTION IS GOING TO OCCUR
       mu=k-1;
    end
     end
    if (mu == 1)   %SO IF MU=1 REACTION ONE WILL OCCUR
    %N=N+1;
    c_m(top_row,1)=c_m(top_row,1)+1; % Result of reation 1 is that NA increases by
one
    end
    if (mu == 2)
    %N=N-1;
    c_m(top_row,1)=c_m(top_row,1)-1;
     end
    if (mu == 3)
    %N=N-1;
    %S=S+1;
    c_m(top_row,1)=c_m(top_row,1)-1;
```

```
c_m(top_row,2)=c_m(top_row,2)+1;
 end
if (mu == 4)
%S=S-1;
c_m(top_row,2)=c_m(top_row,2)-1;
end
if (mu == 5)
%M=M+1;
c_m(top_row,3)=c_m(top_row,3)+1;
end
if (mu == 6)
%M=M-1;
c_m(top_row,3)=c_m(top_row,3)-1;
end
if (mu == 7)
%X=X+1;
c_m(top_row,4)=c_m(top_row,4)+1;
end
if (mu == 8)
%X=X-1;
c_m(top_row,4)=c_m(top_row,4)-1;
end
if (mu == 9)
%R=R+1;
c_m(top_row,5)=c_m(top_row,5)+1;
end
if (mu == 10)
%R=R-1;
c_m(top_row,5)=c_m(top_row,5)-1;
end
if (mu == 11)
%G=G+1;
c_m(top_row,6)=c_m(top_row,6)+1;
end
if (mu == 12)
%G=G-1;
c_m(top_row,6)=c_m(top_row,6)-1;
end
if (mu == 13)
%P=P+1;
c_m(top_row,7)=c_m(top_row,7)+1;
end
if (mu == 14)
%P=P-1;
```

```
    c_m(top_row,7)=c_m(top_row,7)-1;
    end


    %---RECALCULATE PROPENSITIES (Since you updated molecule numbers in
c_m)---
    a1=ka_NA_ECM*((K_o+(K_PA * c_m(top_row,5) )) ./ (1+(K_inhibit *
c_m(top_row,2)  )));
    a2=kd_NA*(1+(K_turnover* c_m(top_row,7) )) .*  c_m(top_row,1);
    a3=k_mature*(1+(K_contract* c_m(top_row,3) )) .* c_m(top_row,1);
    a4=kd_SA* c_m(top_row,2);
    a5=ka_myo* c_m(top_row,2);
    a6=kd_myo* c_m(top_row,3);
    a7=ka_pax*(PAKo+ c_m(top_row,7) ).*( c_m(top_row,1) - c_m(top_row,4) );
    a8=kd_pax* c_m(top_row,4);
    a9=ka_Rac* c_m(top_row,4);
    a10=kd_Rac*(1+(K_GAP* c_m(top_row,6) )).* c_m(top_row,5);
    a11=ka_GAP* c_m(top_row,2);
    a12=kd_GAP* c_m(top_row,6);
    a13=ka_PAK*( c_m(top_row,4) - c_m(top_row,7 )).* c_m(top_row,5);
    a14=kd_PAK* c_m(top_row,7);

    a_sum=a1+a2+a3+a4+a5+a6+a7+a8+a9+a10+a11+a12+a13+a14; %SUM OF ALL
PROPENSITIES

    %---RECALCULATE DIFFUSION RATES---
    myo_diff = dimension * D_myo * c_m(top_row,3);
    Rac_diff = dimension * D_Rac * c_m(top_row,5);
    GAP_diff = dimension * D_GAP * c_m(top_row,6);

    diff_sum=myo_diff+Rac_diff+GAP_diff;

    % Need to update r_m
    r_m(top_row,1) = a_sum;
    r_m(top_row,2) = diff_sum;
    r_m(top_row,3) = (a_sum + diff_sum);


    random2=rand(1,1); %Generates a new random number, one new random number
per iteration

    next_time_event=((-log(random2))/(a_sum+diff_sum)) + tau_matrix_ordered(1,1);
```

```
    tau_matrix_ordered(1,1)=next_time_event;  %Insert new next time event for the
row that was on top during this iteration

    tau_matrix_ordered=sortrows(tau_matrix_ordered); % Ordering the queue after
insertion of a new time

    loop_num=loop_num+1;

    %---THIS WRITES THE SPECIFIED DATA POINTS (every step in tau as
specified)
    tau_step=tau-last_tau;
    if tau_step > data_write_frequency_tau
      row_num_point=row_num_point+1;
      NA_results(row_num_point,:)  = [c_m(:,1)'];
      SA_results(row_num_point,:)  = [c_m(:,2)'];
      Myo_results(row_num_point,:) = [c_m(:,3)'];
      Pax_results(row_num_point,:) = [c_m(:,4)'];
      Rac_results(row_num_point,:) = [c_m(:,5)'];
      GAP_results(row_num_point,:) = [c_m(:,6)'];
      Pak_results(row_num_point,:) = [c_m(:,7)'];
      progress_matrix(row_num_point,:) = [loop_num tau];
      last_tau=tau;
    end



  else
      % ---DIFFUSION EVENT OCCURS---
      diffusion_count=diffusion_count+1;
      sum(1)=0;
      sum(2)=0;
      sum(3)=0;
      sum(4)=0;

      tau=tau_matrix_ordered(1,1) % This is used when storing the model data

      myo_diff = dimension * D_myo * c_m(top_row,3);
      Rac_diff = dimension * D_Rac * c_m(top_row,5);
      GAP_diff = dimension * D_GAP * c_m(top_row,6);

      diff_sum = myo_diff + Rac_diff + GAP_diff;

      yr2 = random1 * diff_sum;
```

```
% A random number is used to determine the direction of diffustion based on the
connectivity matrix
% There are "dimension" directions that each molecule can diffuse
one_to_dimension_number=round((0.5+(dimension*random1))); % This will
generate an integer between 1 and dimension

diff_direction= conn_matrix(top_row,one_to_dimension_number); %This tells
you in which subvolume it will diffuse


sum(2)=sum(1)+myo_diff;
sum(3)=sum(2)+Rac_diff;
sum(4)=sum(3)+GAP_diff;

for k=2:4
  if (sum(k) >= yr2) & (sum(k-1) < yr2) %THIS DETERMINES WHICH
MOLECULE IS GOING TO DIFFUSE
     mu=k-1;
  end
end

if (mu == 1)   %SO IF MU=1 DIFFUSION ONE WILL OCCUR
%Myo will diffuse;
c_m(top_row,3)=c_m(top_row,3)-1; %This says that the Myo diffused away from
active subvolume
c_m(diff_direction,3)=c_m(diff_direction,3)+1; %This says that Myo diffused
into the neighbor subvolume
end

if (mu == 2)
%Rac will diffuse;
c_m(top_row,5)=c_m(top_row,5)-1;
c_m(diff_direction,5)=c_m(diff_direction,5)+1;
end

if (mu == 3)
%GAP will diffuse;
c_m(top_row,6)=c_m(top_row,6)-1;
c_m(diff_direction,6)=c_m(diff_direction,6)+1;
end

% Since the count of molecules was updated, we also need to update the diffusion
rates
```

```
% And we need to do this in both the active subvolume and also the subvolume
that molecules diffused into


%---RECALCULATE PROPENSITIES (Since you updated molecule numbers in
c_m)---
a1_a=ka_NA_ECM*((K_o+(K_PA * c_m(top_row,5) )) ./ (1+(K_inhibit *
c_m(top_row,2)  )));
a2_a=kd_NA*(1+(K_turnover* c_m(top_row,7) )) .*  c_m(top_row,1);
a3_a=k_mature*(1+(K_contract* c_m(top_row,3) )) .* c_m(top_row,1);
a4_a=kd_SA* c_m(top_row,2);
a5_a=ka_myo* c_m(top_row,2);
a6_a=kd_myo* c_m(top_row,3);
a7_a=ka_pax*(PAKo+ c_m(top_row,7) ).*( c_m(top_row,1) - c_m(top_row,4) );
a8_a=kd_pax* c_m(top_row,4);
a9_a=ka_Rac* c_m(top_row,4);
a10_a=kd_Rac*(1+(K_GAP* c_m(top_row,6) )).* c_m(top_row,5);
a11_a=ka_GAP* c_m(top_row,2);
a12_a=kd_GAP* c_m(top_row,6);
a13_a=ka_PAK*( c_m(top_row,4) - c_m(top_row,7 )).* c_m(top_row,5);
a14_a=kd_PAK* c_m(top_row,7);


a_sum_active=a1_a+a2_a+a3_a+a4_a+a5_a+a6_a+a7_a+a8_a+a9_a+a10_a+a11_a+a1
2_a+a13_a+a14_a;

a1_n=ka_NA_ECM*((K_o+(K_PA * c_m(diff_direction,5) )) ./ (1+(K_inhibit *
c_m(diff_direction,2)  )));
a2_n=kd_NA*(1+(K_turnover* c_m(diff_direction,7) )) .*  c_m(diff_direction,1);
a3_n=k_mature*(1+(K_contract* c_m(diff_direction,3) )) .*
c_m(diff_direction,1);
a4_n=kd_SA* c_m(diff_direction,2);
a5_n=ka_myo* c_m(diff_direction,2);
a6_n=kd_myo* c_m(diff_direction,3);
a7_n=ka_pax*(PAKo+ c_m(diff_direction,7) ).*( c_m(diff_direction,1) -
c_m(diff_direction,4) );
a8_n=kd_pax* c_m(diff_direction,4);
a9_n=ka_Rac* c_m(diff_direction,4);
a10_n=kd_Rac*(1+(K_GAP* c_m(diff_direction,6) )).* c_m(diff_direction,5);
a11_n=ka_GAP* c_m(diff_direction,2);
a12_n=kd_GAP* c_m(diff_direction,6);
a13_n=ka_PAK*( c_m(diff_direction,4) - c_m(diff_direction,7 )).*
c_m(diff_direction,5);
a14_n=kd_PAK* c_m(diff_direction,7);
```

```
a_sum_neighbor=a1_n+a2_n+a3_n+a4_n+a5_n+a6_n+a7_n+a8_n+a9_n+a10_n+a11_n
+a12_n+a13_n+a14_n;


    %---RECALCULATE DIFFUSION RATES---
    myo_diff_active = dimension * D_myo * c_m(top_row,3);
    Rac_diff_active = dimension * D_Rac * c_m(top_row,5);
    GAP_diff_active = dimension * D_GAP * c_m(top_row,6);

    myo_diff_neighbor = dimension * D_myo * c_m(diff_direction,3);
    Rac_diff_neighbor = dimension * D_Rac * c_m(diff_direction,5);
    GAP_diff_neighbor = dimension * D_GAP * c_m(diff_direction,6);

    diff_sum_active=myo_diff_active+Rac_diff_active+GAP_diff_active;
    diff_sum_neighbor=myo_diff_neighbor+Rac_diff_neighbor+GAP_diff_neighbor;


    % Need to update r_m
    r_m(top_row,1) = a_sum_active;
    r_m(top_row,2) = diff_sum_active;
    r_m(top_row,3) = (a_sum_active + diff_sum_active);

    r_m(diff_direction,1) = a_sum_neighbor;
    r_m(diff_direction,2) = diff_sum_neighbor;
    r_m(diff_direction,3) = (a_sum_neighbor + diff_sum_neighbor);


    random2=rand(1,1);
    random3=rand(1,1);


    next_tau_event_active=((-log(random2))/(a_sum_active+diff_sum_active));
    next_tau_event_neighbor=((-
log(random3))/(a_sum_neighbor+diff_sum_neighbor));


    tau_matrix_ordered_by_subvolume=sortrows(tau_matrix_ordered, [2]); % This
sorts the tau_matrix by the subvolume number

    % Enter the new event times into the tau_matrix
```

```
        % Remeber that the next tau events are added to the current time in the matrix so
you get next time event
        tau_matrix_ordered_by_subvolume(top_row,1)=next_tau_event_active +
tau_matrix_ordered_by_subvolume(top_row,1);
        tau_matrix_ordered_by_subvolume(diff_direction,1)=next_tau_event_neighbor +
tau_matrix_ordered_by_subvolume(diff_direction,1);

        % Sort based on the next event times
        tau_matrix_ordered=sortrows(tau_matrix_ordered_by_subvolume); % Ordering
the queue after insertion of the new times

        top_row = tau_matrix_ordered(1,2);

        loop_num=loop_num+1;


    %---THIS WRITES THE SPECIFIED DATA POINTS (every step in tau as
specified)
    tau_step=tau-last_tau;
    if tau_step > data_write_frequency_tau
      row_num_point=row_num_point+1;
      NA_results(row_num_point,:)  = [c_m(:,1)'];
      SA_results(row_num_point,:)  = [c_m(:,2)'];
      Myo_results(row_num_point,:) = [c_m(:,3)'];
      Pax_results(row_num_point,:) = [c_m(:,4)'];
      Rac_results(row_num_point,:) = [c_m(:,5)'];
      GAP_results(row_num_point,:) = [c_m(:,6)'];
      Pak_results(row_num_point,:) = [c_m(:,7)'];
      progress_matrix(row_num_point,:) = [loop_num tau];
      last_tau=tau;
    end

   end

end   %end of the (while time<timelimit) loop

%-----MAKE MATRIXES FOR EACH VARIABLE WITH LOOP NUMBER AND
TAU VALUE-----
NA_results_write   = [NA_results  progress_matrix];
SA_results_write   = [SA_results  progress_matrix];
Myo_results_write  = [Myo_results progress_matrix];
Pax_results_write  = [Pax_results progress_matrix];
Rac_results_write  = [Rac_results progress_matrix];
GAP_results_write  = [GAP_results progress_matrix];
```

```
Pak_results_write  = [Pak_results progress_matrix];

%-----WRITE MATRIX OF RESULTS FOR EACH VARIABLE-----
wk1write('NA_results', NA_results_write);
wk1write('SA_results', SA_results_write);
wk1write('Myo_results', Myo_results_write);
wk1write('Pax_results', Pax_results_write);
wk1write('Rac_results', Rac_results_write);
wk1write('GAP_results', GAP_results_write);
wk1write('Pak_results', Pak_results_write);


NA_max  = max(max(NA_results))   %  Finds maximum value in the entire matrix
SA_max  = max(max(SA_results))
Myo_max = max(max(Myo_results))
Pax_max = max(max(Pax_results))
Rac_max = max(max(Rac_results))
GAP_max = max(max(GAP_results))
Pak_max = max(max(Pak_results))


%----- MAKING A MOVIE--------
num_written_points=size(progress_matrix);
numframes = (num_written_points(1,1));     % This specifies how many frames you
want to make the movie from
num_frames_per_second = 30;
dur = numframes / num_frames_per_second;
%  The AVIFILE function creates a new Audio Video Interleaved (AVI) file.
%  We specify its name, and we also set the value of "FPS", which is the
%  rate at which we will display frames (individual snapshots) per second.
aviobj = avifile ( 'results_movie.avi', 'fps', num_frames_per_second , 'compression',
'Cinepak', 'quality', 100 );



for i =  1 : numframes

    subplot(3,1,1); bar(NA_results(i,:),'b')       % This creates a bar graph of particular
line of data
    ylabel('NA')                              % This specifies the limits on the Y axes
    set(gca,'YLim',[0,NA_max],'Layer','top')
    set(gca,'XLim',[0,subvolumes+1],'Layer','top')

    subplot(3,1,2); bar(SA_results(i,:),'r')
```

```
    ylabel('SA')
    set(gca,'YLim',[0,SA_max],'Layer','top')
    set(gca,'XLim',[0,subvolumes+1],'Layer','top')

    subplot(3,1,3); bar(Rac_results(i,:),'g')
    xlabel('subvolume')
    ylabel('Rac')
    set(gca,'YLim',[0,Rac_max],'Layer','top')
    set(gca,'XLim',[0,subvolumes+1],'Layer','top')
    i                                   % Shows current i in the command window so you can
track the progress
    frame = getframe ( gcf );                   % Gets the current frame
                                %     gcf --> you will get the whole figure (with axes)
                                %     gca --> you will get only what is within the axes
   aviobj = addframe ( aviobj, frame );    % Adds the current frame to the video
end

aviobj = close ( aviobj );   % Command to complete the movie

%----- END OF MOVIE MAKING -----



time_end=clock; % This is the time the code stoped running
c_m
r_m
loop_num
reaction_count
diffusion_count
run_time=time_end-time_start
run_time_minutes=(run_time(1,3)*24*60) + (run_time(1,4)*60) + run_time(1,5) +
(run_time(1,6)/60)

tau_matrix_ordered

par_matrix = [Gn;
            En;
            In;
            Cn;
            Es;
            Gx;
            Po;
            Cr;
            Kp;
```

```
        Lm;
        Lr;
        Lg;
        kd_NA;
        kd_SA;
        kd_myo;
        kd_pax;
        kd_GAP;
        kd_PAK;
        kd_Rac;
        K_turnover;
        K_o;
        K_PA;
        K_contract;
        K_GAP;
        loop_num;
        tau_matrix_ordered(1,1);
        reaction_count;
        diffusion_count;
        run_time_minutes;];

wk1write('Parameter_matrix', par_matrix);
```